Supplemental Information

Perfluoroalkylated amphiphilic porphyrin nanomicelle for improved photodynamic therapeutic anti-tumour efficacy through stability enhancement and O_2 enrichment

Dan-Wei Zhang[1*], Danying Ma[1], Congying Guo[1], Zhuo Lei[2], Yajie Zhu[2], Rui Gao[1], Hui Wang[1], Jia Tian[2], Wei Zhou[1] & Zhan-Ting Li[1,2*]

[1]*Department of Chemistry, Fudan University, 2205 Songhu Road, Shanghai 200438, China*
[2]*State Key Laboratory of Organometallic Chemistry, Shanghai Institute of Organic Chemistry, Chinese Academy of Sciences, University of Chinese Academy of Sciences, 345 Lingling Road, Shanghai 200032, China*

Emails: zhangdw@fudan.edu.cn (D.-W. Zhang), ztli@fudan.edu.cn (Z.-T. Li)

General methods and materials. All the reagents and solvents were commercially available and used as received. ^{1}H NMR spectra were recorded with an AVANCE III HD 400 MHz spectrometer (Bruker) in the indicated solvents at 25 °C. Chemical shifts were referenced to the residual solvent peaks. High-resolution mass spectra (HR-MS) were recorded on a Bruker MicrOTOF II analyzer. Dynamic light scattering (DLS) experiments were conducted on a Malvern Zetasizer Nano ZS90 using a monochromatic coherent He-Ne laser (633 nm) as light source and a detector that detected the scattered light at an angle of 90°. Bright-field TEM images were obtained using a JEOL JEM 1400 microscope operating at 80 kV with a Gatan Orius SC200 CCD camera. Fluorescent spectra were recorded on a VARIAN CARY Eclipse Fluorescence Spectrophotometer. UV-visible absorption spectra were recorded with a PerkinElmer LAMBDA 650 UV/Vis/NIR spectrometer. Fluorescent microscopic experiments were performed on the FluoView FV1000, Olympus fluorescent microscope. Flow cytometric experiments were conducted with a CytoFlex LX flow cytometry system. Dissolved oxygen meter (WLDO-300, Shanghai Water Science and Technology Co., Ltd.) was used to measure the changes in oxygen concentration in the solution. Fetal bovine serum (FBS), 1640 Medium, and DMEM Medium were purchased from Thermo Fisher Scientific.

Dynamic light scattering experiments. For the determination of the hydrodynamic diameters by dynamic light scattering experiments, the solutions of **TSCnP** (n = 5-8) and **F-TSCnP** (n = 5-8) were prepared in phosphate-buffered saline (PBS, 10 mM, pH = 7.4) to form a series of concentrations (from 10 μM to 100 μM). The samples were left to stand at 25 °C for 24 h before measurement. All the samples were tested for 100 duplications for the final size distribution. The reported outcomes are average of three replicative measurements.

Transmission electron microscope experiments. For the morphology observation by transmission electron microscope experiments, the solutions of **F-TSCnP** (n = 5-8) and **TSCnP** (n = 5-8) (all 10 μM) were prepared in deionized water or phosphate-buffered saline (PBS, 10 mM, pH = 7.4). The solutions were left to stand at 25 °C for 24 h and then dropped (~4 μl) onto a copper 400 mesh TEM grid with a carbon-film support. Negatively stained samples were prepared using a 1% aqueous solution of uranyl acetate.

Cell Culture. H9C2 and MCF-7 cell lines were incubated in DMEM medium with 10% FBS and 1% penicillin streptomycin at 37 °C in a humidified atmosphere containing 5% CO_2. B16-F10 cell lines were incubated in 1640 medium with 10% FBS and 1% penicillin streptomycin at 37 °C in a humidified atmosphere containing 5% CO_2.

Confocal laser scanning microscopy (CLMS). For CLMS observations of the cell uptake and intracellular distribution of **TSCnP** (n = 5-8) and **F-TSCnP** (n = 5-8), B16-F10 or MCF-7 cells (10^5 cells per dish) were seeded in coverglass bottom dishes (35 mm × 10 mm), and treated with 20 μM **F-TSCnP** (n = 5-8) in the completed medium as the experimental group, 20 μM **TSCnP** (n = 5-8) in the completed medium as the

positive control group and the pure completed medium as negative control group. After incubation for 4 h, the cells were softly washed twice to remove excessive porphyrin molecules. The cell nuclei were then dyed by 10 μg/mL bisBenzimide H 33342 trihydrochloride (Hoechst 33342) for additional 20 min, followed by washing with PBS twice to remove excessive Hoechst 33342. PBS solution (1 mL) was then added to each dish, and the cells were visualized under a confocal laser scanning microscope (FluoView FV1000, Olympus). The fluorescence images were taken under 40 × objective.

For CLSM observations of intracellular $^1O_2$ generation under laser irradiation, MCF-7 cells (10^5 cells per dish) were seeded in coverglass bottom dishes (35 mm × 10 mm), and treated with 20 μM **F-TSC8P** in the completed medium as the experimental group and 20 μM **TSC8P** in the completed medium as the control group. After incubation for 4 h, the cells were softly washed twice to remove excessive porphyrin molecules. The cell nuclei were then dyed by 10 μg/mL bisBenzimide H 33342 trihydrochloride (Hoechst 33342) for additional 20 min, followed by washing with PBS twice to remove excessive Hoechst 33342. Then, the intracellular reactive oxygen species were probed with serum-free medium containing 10 μg/mL 2',7'-Dichlorodihydrofluorescein diacetate (DCFH-DA) for another 0.5 h, then washed with PBS twice to remove excessive DCFH-DA, followed by laser irradiation (655 nm, 200 mW/cm^2, 12 J/cm^2, 1 min) for the irradiation group and light tight incubation for the non-irradiation group. PBS solution (1 mL) was then added to each dish. Finally, the cells were visualized under a confocal laser scanning microscope (FluoView FV1000, Olympus). The fluorescence images were taken under 40 × objective.

Flow cytometric uptake analyses. For quantitative cell uptake analyses of **TSCnP** (n = 5-8) and **F-TSCnP** (n = 5-8) by flow cytometric, B16-F10 and MCF-7 cells were seeded at 5 × 10^5 cells per well in 6-well plate and further cultured for 24 h. Then, the culture medium was removed and culture medium containing 20 μM of different kinds of porphyrin doses were added. The cells were then cultured for another 4 h and washed with PBS twice. Cells were collected in the darkness. Finally, the fluorescence intensity of the cells was measured by a flow cytometer (CytoFlex LX) with an excitation wavelength of 561 nm and emission wavelength of 675/30 nm. Totally 10,000 cells were tested for each sample.

Dissolved oxygen (DO) detection of F-TSC8P and TSC8P nanoparticles solutions. Using a portable oxygen analyzer and pure PBS (10 mM, pH = 7.4) as control, the oxygen solubility capacity of the **F-TSC8P** and **TSC8P** solutions at the same concentration was tested. According to the reported method,[1] nanoparticle solutions of **F-TSC8P** and **TSC8P** at a concentration of 200 μM were prepared and left to stand for 24 h and then oxygenated for 1 h until oxygen saturation. Subsequently, the solutions (2.5 mL) were slowly poured into deoxygenated PBS (10 mL, 10 mM, pH = 7.4) at a volume ratio of 1:4. The dissolved oxygen meter (WLDO-300, Shanghai Water Science and Technology Co., Ltd.) was used to measure the changes in oxygen concentration in the solution with the probe to touch the bottom of the solution, and the oxygen

concentration of the mixed solution was monitored in real-time with readings recorded every 15 s until it was stabilized.

Detection of in vitro single oxygen generation rate of F-TSC8P and TSC8P. Commercial ABDA and SOSG were utilized as tracer agent to assess $^1O_2$ production efficiencies of various samples.[2,3] Specifically, each sample and ABDA were dispersed in 3 mL of deionized water, with final concentrations of 10 μM and 100 μM, respectively. Subsequently, the mixed solution was irradiated with 655 nm laser at a power of 200 mW/cm^2. The $^1O_2$ generation efficiency was measured by monitoring the UV-vis absorbance change of ABDA at 378 nm at different irradiation time intervals. While, each sample and SOSG were dispersed in 3 mL of deionized water, with final concentrations of 5 μM and 5 μM, respectively. Subsequently, the mixed solution was irradiated with 655 nm laser at a power of 200 mW/cm^2. The $^1O_2$ generation efficiency was measured by monitoring the FL intensity change of SOSG at 378 nm at different irradiation time intervals.

In vitro photo cytotoxicity assay of F-TSC8P and TSC8P. Cytotoxicity was determined using the Cell Counting Kit-8 (CCK-8) assay in B16-F10 or MCF-7 cell lines [2]. Cells growing in the log phase were seeded into 96-well cell culture plate at 2×10^4 per well and then incubated under 5% CO_2 at 37 °C for 24 h. Completed medium of the porphyrin dose (100 μL/well) of different concentrations were added to the wells of the treatment group. Pure completed medium (100 μL/well) was added to the well of the negative control group. The cells were incubated under 5% CO_2 at 37 °C for 24 h. Then, for the group not treated by laser irradiation, the cells were continuously cultured in the dark under 5% CO_2 for 24 h at 37 °C. While, for the group treated by laser irradiation, the cells were irradiated under 655 nm laser (50 mW/cm^2, 60 J/cm^2) for 20 min, which was following by incubation under 5% CO_2 at 37 °C for additional 24 h. Finally, 100 μL CCK-8 was added to each well of all the 96-well assay plates and incubated under 5% CO_2 at 37 °C for an additional 1 h. The absorbance (A value) of each well was measured at 450 nm using a microplate reader (Bio-Tek, Synergy H1, USA). The viability of cell growth was calculated using the formula: cell viability (%) = (mean of A value of treatment group/mean of A value of control) ×100%.

In vivo photo cytotoxicity assay of F-TSC8P and TSC8P. For the evaluations of photodynamic anti-tumor activity of **F-TSC8P** and **TSC8P**,[2] 20 BALB/c nude mice (18-22 g, n = 5, female) were individually weighed. B16-F10 cells were suspended in PBS and implanted intracutaneously into the right underarm skin of the mice in 100 μL (8×10^4 cells/site). Tumor bearing female nude mice were reset to 4 groups at random (n = 5) after tumor volumes reached ~ 4 mm^3, which was followed by injection of 100 μL of **F-TSC8P** or **TSC8P** at a dosage of 4 mg porphyrins/kg, with PBS (10 mM, pH = 7.4) as control. After standing for 4 h, mice in control group, **F-TSC8P**-irradiation group, and **TSC8P**-irradiation group were irradiated under a 655 nm laser for 10 min at a photodensity of 0.5 W/cm^2. All the groups were left for daily observations. Tumor sizes were measured by digital calipers every day. Tumor volumes were calculated as (tumor length) × (tumor width)^2/2. Body weights of mice were also measured every day

and normalized to their initial weights. After 11 days of observations, the mice were euthanized and both organs and tumors were collected for all groups. The histopathological sections of collected organs and tumors were prepared and stained with hematoxylin and eosin (H&E), which was subjected to optical microscopic imaging. The histopathological sections of collected tumors were also stained with deoxynucleotidyl transferase-mediated nick-end labeling (TUNEL), and Ki-67, and subjected to fluorescence microscopic imaging.

Maximum tolerated dose (MTD) evaluations for F-TSC8P. Totally 24 ICR mice (19-24 g, n = 6, half female and male) were individually weighed and randomly divided into four groups. In the control group, mice were intravenously injected with 0.5 mL saline. For another three experimental groups, **F-TSC8P** was intravenously injected with the doses of 20, 30 and 40 mg/kg. Body weights of the mice was monitored twice a day at defined time and their general behaviors were observed and recorded. After 14 days, the mice were euthanized and the major organs collected for both control group and high-dose group. The histopathological sections of the collected organs were prepared and stained with hematoxylin and eosin (H&E), and subjected optical microscopic imaging.

Synthesis and characterization

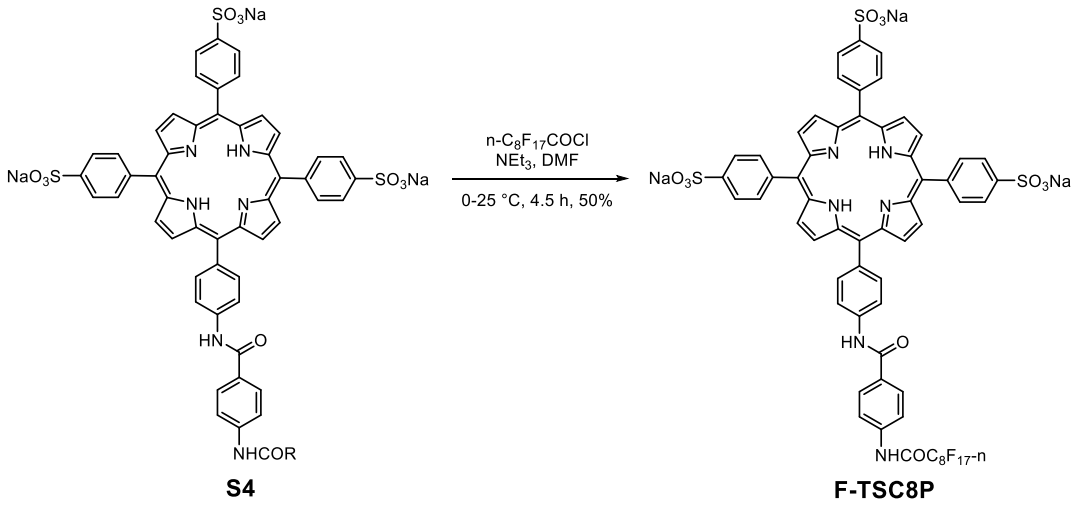

Compound F-TSC8P. Under a nitrogen atmosphere, compound **S4** [2] (53 mg, 0.05 mmol) was added into a 50 mL three-neck flask containing *N*,*N*-dimethylformamide (DMF) (8 mL) and triethylamine (0.1 mL). The mixture was stirred at room temperature to allow the solid to dissolve and then cooled in an ice bath. To the solution was then added perfluorononanoyl chloride (70 μL, 2.9 mmol), and the mixture was stirred for 30 min and then for 4 h at room temperature. The mixture was then concentrated with a rotavapor. To the resulting residue was added methanol and ethyl acetate (1:1, 1 mL). The purple precipitate formed was collected by centrifugation and then recrystallized by methanol and dimethyl chloride (1:1) to afford **F-TSC8P** as a purple solid (38 mg, 50%). ^{1}H NMR (400 MHz, DMSO-d_6) δ 11.60 (s, 1H), 10.70 (s, 1H), 8.91 (d, J = 4.8

Hz, 2H), 8.86 (s, 6H), 8.30–8.12 (m, 12H), 8.04 (d, J = 7.9 Hz, 6H), 7.93 (d, J = 8.7 Hz, 2H), –2.91 (s, 2H). ^{19}F NMR (471 MHz, DMSO-d_6) δ –80.11 (t, J = 9.9 Hz), –117.93 (t, J = 12.5 Hz), –121.20, –121.33~–121.68 (m), –121.89, –122.35, –125.48~–125.77 (m). ^{13}C NMR (126 MHz, DMSO-d_6) δ 165.59, 155.84, 148.42, 141.73, 139.70, 139.56, 136.85, 135.14, 134.19, 132.74, 129.37, 124.68, 121.42, 120.53, 120.16, 120.08, 119.15. HRMS: calcd for $C_{60}H_{33}F_{17}N_6O_{11}S_{32}$ $[M+H]^{2+}$ 716.0549, found 716.0583.

F-TSCnP (n = 5~7). The three compounds were prepared from the respective reaction of compound **S4** and the corresponding perfluoroacyl chloride according to similar procedures. **F-TSC5P:** purple solid, 50%. ^{1}H NMR (400 MHz, DMSO-d_6) δ 11.59 (s, 1H), 10.69 (s, 1H), 8.88 (s, 8H), 8.33–8.12 (m, 13H), 8.04 (d, J = 7.6 Hz, 6H), 7.93 (d, J = 8.3 Hz, 2H), –2.91 (s, 2H). ^{19}F NMR (471 MHz, DMSO-d_6) δ –80.15 (t, J = 8.1 Hz), –118.00 (t, J = 11.9 Hz), –122.21 (dq, J_1 = 12.1 Hz, J_2 = 11.2 Hz), –125.74 (t, J = 14.9 Hz). ^{13}C NMR (126 MHz, DMSO-d_6) δ 165.60, 156.06, 155.85, 148.37, 141.75, 139.67, 139.56, 136.86, 135.13, 134.19, 132.73, 129.36, 124.68, 121.42, 120.53, 120.15, 120.07, 119.17. HRMS: calcd for $C_{57}H_{33}F_{11}N_6O_{11}S_{32}$ $[M+H]^{2+}$ 641.0597, found 641.0612. **F-TSC6P:** purple solid, 45%. ^{1}H NMR (400 MHz, DMSO-d_6) δ 11.59 (s, 1H), 10.69 (s, 1H), 8.88 (d, J = 18.0 Hz, 8H), 8.21 (dd, J_1 = 24.6 Hz, J_2 = 8.2 Hz, 13H), 8.04 (d, J = 7.7 Hz, 6H), 7.93 (d, J = 8.3 Hz, 2H), –2.90 (s, 2H). ^{19}F NMR (471 MHz, DMSO-d_6) δ –80.13 (t, J = 9.8 Hz), –117.95 (t, J = 12.6 Hz), –121.44, –121.96, –122.45, –125.64. ^{13}C NMR (126 MHz, DMSO-d_6) δ 148.47, 141.70, 135.14, 134.18, 129.37, 124.67, 121.41, 120.17, 119.14, 40.50, 40.33, 40.17, 40.00, 39.83, 39.66, 39.50. HRMS: calcd for $C_{58}H_{33}F_{13}N_6O_{11}S_{32}$ $[M+H]^{2+}$ 666.0581, found 666.0607. **F-TSC7P:** purple solid, 48%. ^{1}H NMR (400 MHz, DMSO-d_6) δ 11.59 (s, 1H), 10.69 (s, 1H), 8.88 (s, 8H), 8.31–8.14 (m, 12H), 8.03 (s, 6H), 7.93 (d, J = 8.6 Hz, 2H), –2.91 (s, 2H). ^{19}F NMR (471 MHz, DMSO-d_6) δ –80.12 (t, J = 9.9 Hz), –117.92 (t, J = 12.8 Hz), –121.22, –121.66, –121.91, –122.35, –125.62 (t, J = 17.5 Hz). ^{13}C NMR (126 MHz, DMSO-d_6) δ 165.58, 155.83, 148.43, 141.72, 139.69, 139.55, 136.86, 135.14, 134.18, 132.74, 129.37, 124.67, 121.40, 120.53, 120.16, 120.08, 119.14. HRMS: calcd for $C_{59}H_{33}F_{15}N_6O_{11}S_{32}$ $[M+H]^{2+}$: 691.0565, found 691.0577.

S4 **TSC8P**

Compound TSC8P. Under a nitrogen atmosphere, compound **S4** (53 mg, 0.05 mmol) was added into a 50 mL three-neck flask containing DMF (8 mL) and triethylamine (0.1 mL). The mixture was stirred at room temperature to allow the solid to dissolve and then cooled in an ice bath. To the solution was then added nonanoyl chloride (53 mg, 2.9 mmol), and the mixture was stirred for 30 min and then for 12 h at room temperature. The mixture was then concentrated with a rotavapor. To the resulting residue was added methanol and ethyl acetate (1:1, 1 mL). The purple precipitate formed was collected by centrifugation and then recrystallized by methanol and dimethyl chloride (1:1) to afford **TSC8P** as a purple solid (33 mg, 55%). ^{1}H NMR (400 MHz, DMSO-d_6) δ 10.56 (s, 1H), 10.23 (s, 1H), 8.88 (d, J = 21.7 Hz, 8H), 8.30–8.14 (m, 10H), 8.07 (dd, J_1 = 18.1 Hz, J_2 = 7.9 Hz, 8H), 7.82 (d, J = 8.2 Hz, 2H), 2.38 (t, J = 7.4 Hz, 2H), 1.70–1.58 (m, 2H), 1.30 (d, J = 14.6 Hz, 10H), 0.88 (t, J = 6.0 Hz, 3H), –2.91 (s, 2H).^{13}C NMR (126 MHz, DMSO-d_6) δ 171.77, 165.31, 147.93, 142.42, 141.23, 139.35, 136.12, 134.56, 133.64, 129.10, 128.76, 124.15, 120.08, 119.62, 119.53, 118.59, 118.24, 36.49, 31.24, 28.75, 28.67, 28.57, 24.99, 22.05, 13.93. HRMS: calcd for $C_{60}H_{50}N_6O_{11}S_3$ $[M+H]^{2+}$ 563.1355, found 563.1350.

TSCnP (n = 5~7). The three compounds were prepared from the respective reaction of compound **S4** and the corresponding acyl chloride according to similar procedures. **TSC5P:** purple solid, 60%. ^{1}H NMR (400 MHz, DMSO-d_6) δ 10.55 (s, 1H), 10.21 (s, 1H), 8.97–8.78 (m, 8H), 8.30–8.14 (m, 10H), 8.07 (dd, J_1 = 19.8 Hz, J_2 = 8.4 Hz, 8H), 7.82 (d, J = 8.7 Hz, 2H), 2.39 (t, J = 7.5 Hz, 2H), 1.65 (q, J = 7.3 Hz, 2H), 1.34 (dq, J_1 = 7.6 Hz, J_2 = 3.4 Hz, 4H), 0.96–0.87 (m, 3H), –2.91 (s, 2H). ^{13}C NMR (126 MHz, DMSO-d_6) δ 171.83, 165.37, 147.91, 142.46, 141.29, 139.39, 136.17, 134.63, 133.71, 129.15, 128.82, 124.20, 120.13, 119.67, 119.57, 118.63, 118.28, 36.50, 30.93, 24.72, 21.94, 13.91. HRMS: calcd for $C_{57}H_{44}N_6O_{11}S_3$ $[M+H]^{2+}$ 542.1120, found 542.1115. **TSC6P:** purple, 65%. ^{1}H NMR (400 MHz, DMSO-d_6) δ 10.58 (s, 1H), 10.23 (s, 1H), 8.94-8.88 (m, 8H), 8.25-8.23 (m, 10H), 8.08 (d, J = 8.1 Hz, 8H), 7.83 (d, J = 8.3 Hz, 2H), 2.38 (t, J = 7.5 Hz, 2H), 1.64 (d, J = 7.4 Hz, 2H), 1.30 (s, 6H), 0.89 (t, J = 6.1 Hz, 3H), –2.90 (s, 2H). ^{13}C NMR (126 MHz, DMSO-d_6) δ 172.33, 165.87, 148.26, 148.23, 142.93, 141.84, 141.81, 139.86, 136.63, 135.08, 134.18, 129.60, 129.27, 124.69, 120.63, 120.12, 120.01, 119.13, 118.79, 37.00, 31.51, 28.81, 25.45, 22.46, 14.41. HRMS: calcd for $C_{58}H_{46}N_6O_{11}S_3$ $[M+H]^{2+}$ 549.1193, found 549.1197. **TSC7P:** purple solid, 58%. ^{1}H NMR (400 MHz, DMSO-d_6) δ 10.56 (s, 1H), 10.22 (s, 1H), 8.90-8.88 (m, 8H), 8.31–8.15 (m, 10H), 8.07 (t, J = 7.6 Hz, 8H), 7.83 (d, J = 8.2 Hz, 2H), 2.39 (t, J = 7.5 Hz, 2H), 1.64 (s, 2H), 1.33-1.29 (m, 8H), 0.89 (t, J = 6.0 Hz, 3H), –2.90 (s, 2H). ^{13}C NMR (126 MHz, DMSO-d_6) δ 172.29, 165.83, 148.38, 148.36, 142.92, 141.77, 141.73, 139.86, 136.63, 135.08, 134.16, 129.61, 129.27, 124.66, 120.60, 120.13, 120.03, 119.10, 118.76, 37.00, 31.65, 29.13, 28.95, 25.50, 22.55, 14.43. HRMS: calcd for $C_{59}H_{48}N_6O_{11}S_3$ $[M+H]^{2+}$ 556.1271, found 556.1270.

DLS profiles

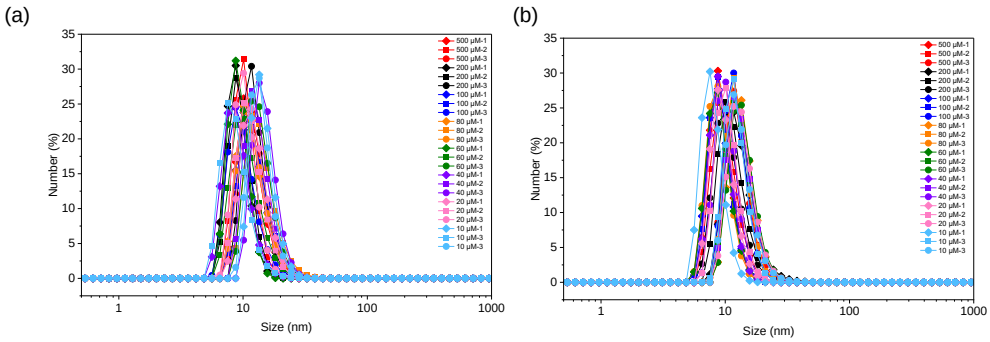

Figure S1. DLS profiles for the evaluation of hydrodynamic diameter (D_H) distribution of **F-TSC8P** (10 μM to 500 μM) in (a) PBS solution (10 mM, pH 7.4) and (b) saline.

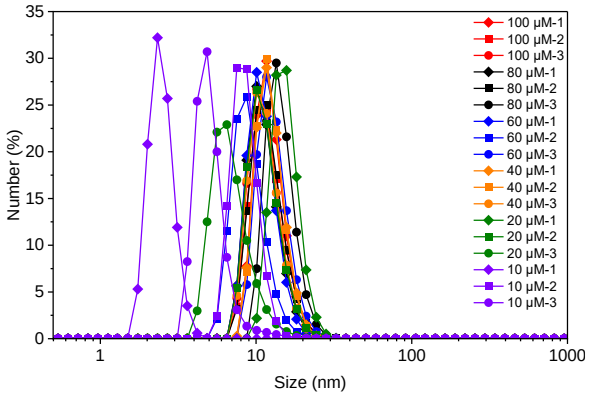

Figure S2. DLS profiles for the evaluation of hydrodynamic diameter (D_H) distribution of **F-TSC7P** (10 μM to 100 μM) in PBS solution (10 mM, pH 7.4).

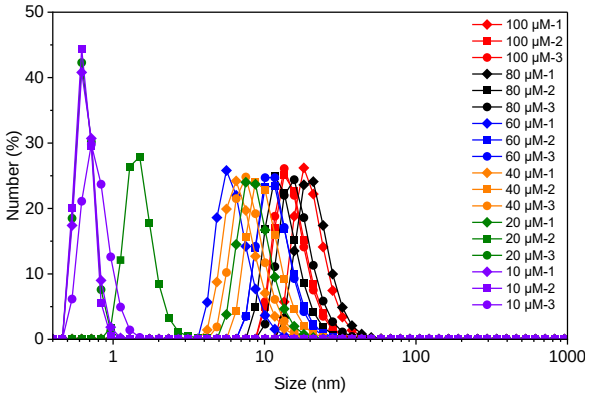

Figure S3. DLS profiles for the evaluation of hydrodynamic diameter (D_H) distribution of **F-TSC6P** (10 μM to 100 μM) in PBS solution (10 mM, pH 7.4).

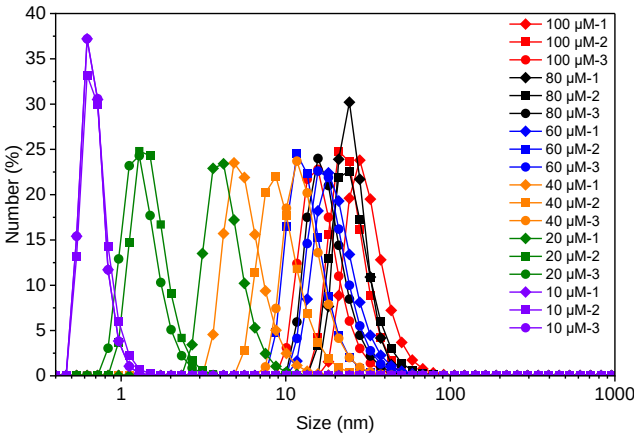

Figure S4. DLS profiles for the evaluation of hydrodynamic diameter (D_H) distribution of **F-TSC5P** (10 μM to 100 μM) in PBS solution (10 mM, pH 7.4).

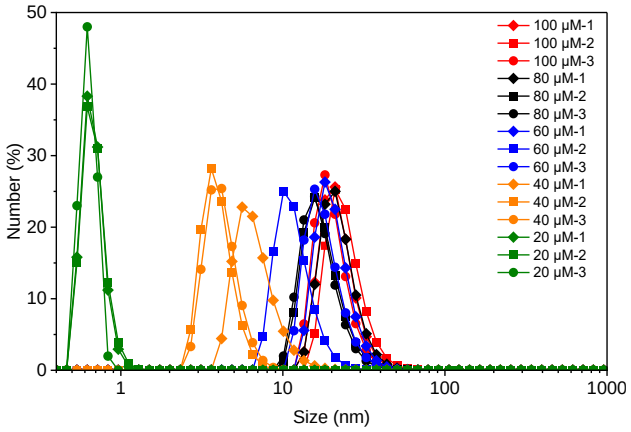

Figure S5. DLS profiles for the evaluation of hydrodynamic diameter (D_H) distribution of **TSC8P** (20 μM to 100 μM) in PBS solution (10 mM, pH 7.4).

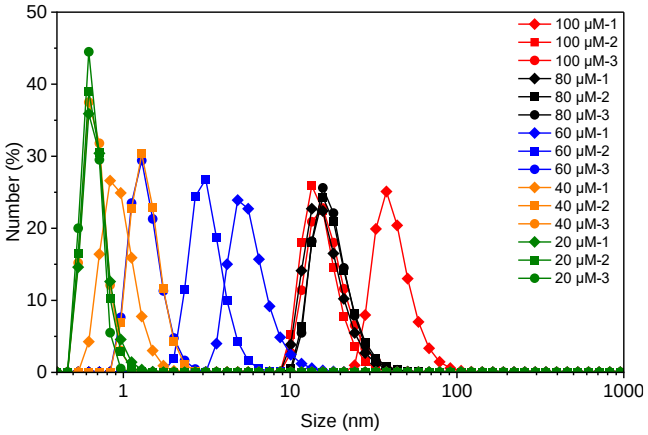

Figure S6. DLS profiles for the evaluation of hydrodynamic diameter (D_H) distribution of **TSC7P** (20 μM to 100 μM) in PBS solution (10 mM, pH 7.4).

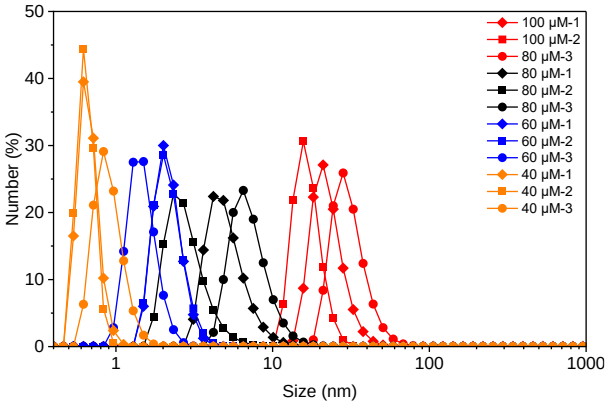

Figure S7. DLS profiles for the evaluation of hydrodynamic diameter (D_H) distribution of **TSC6P** (40 μM to 100 μM) in PBS solution (10 mM, pH 7.4).

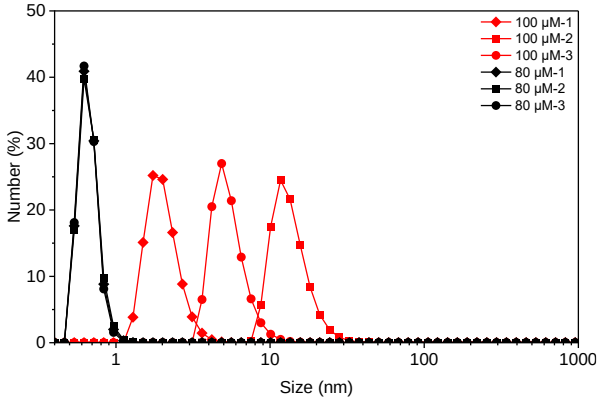

Figure S8. DLS profiles for the evaluation of hydrodynamic diameter (D_H) distribution of **TSC5P** (80 μM to 100 μM) in PBS solution (10 mM, pH 7.4).

Zeta potential profile

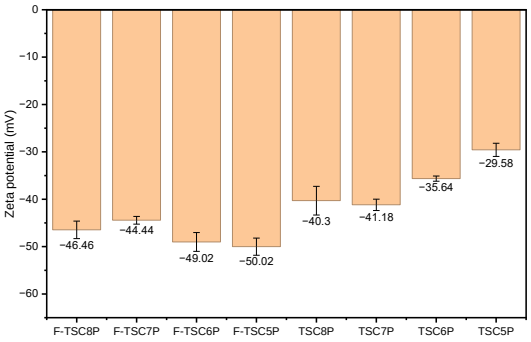

Figure S9. Zeta potential of **F-TSCnP** (n = 5-8) and **TSCnP** (n = 5-8) ([porphyrin] = 0.2 mM) in water. All the solutions were left to stand for 24 h before measurement. Data are presented as mean ± standard deviation. The error bars indicate the standard deviations from five replicative measurements.

TEM images

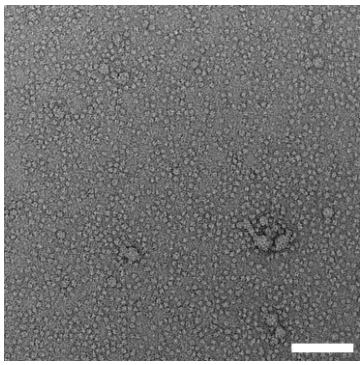

Figure S10. TEM image of **F-TSC8P** in deionized water with negative staining. The sample was prepared by dropping of the solution on an ultrathin carbon film. ([**F-TSC8P**] = 500 μM, scale bar: 100 nm).

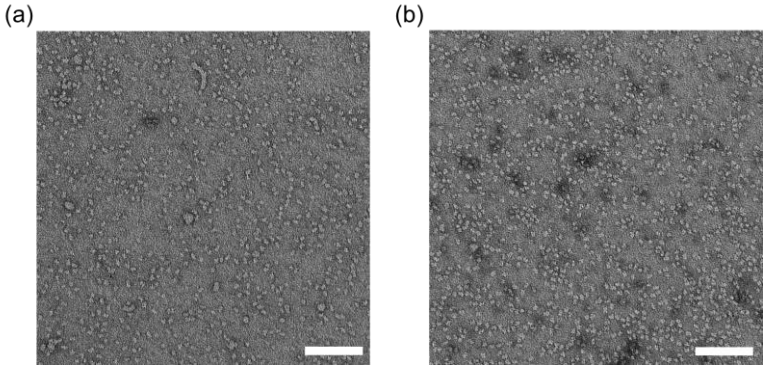

Figure S11. (a) TEM image of **F-TSC7P** in deionized water with negative staining. (b) TEM image of **F-TSC7P** in phosphate-buffered saline (PBS, 10 mM, pH = 7.4) with negative staining. The sample was prepared by dropping of the solution on an ultrathin carbon film. ([**F-TSC7P**] = 500 μM, scale bar: 100 nm).

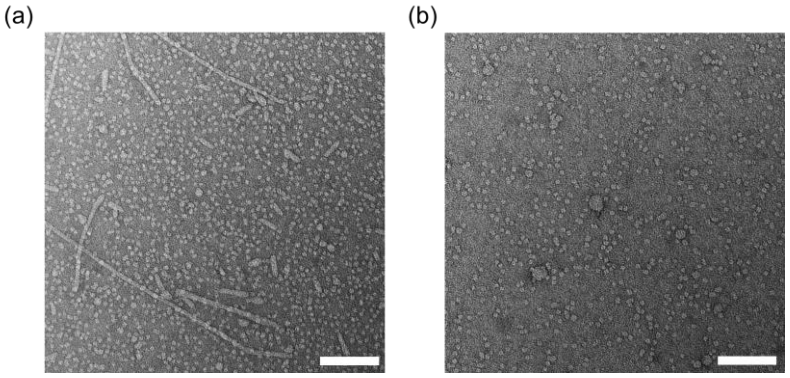

Figure S12. (a) TEM image of **F-TSC6P** in deionized water with negative staining. (b) TEM image of **F-TSC6P** in phosphate-buffered saline (PBS, 10 mM, pH = 7.4) with negative staining. The sample was prepared by dropping of the solution on an ultrathin carbon film. ([**F-TSC6P**] = 500 μM, scale bar: 100 nm).

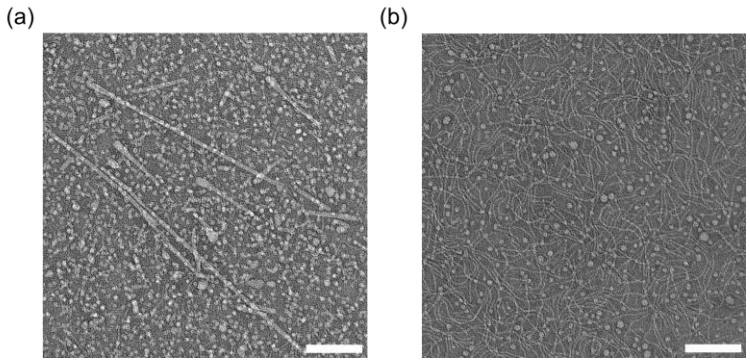

Figure S13. (a) TEM image of **F-TSC5P** in deionized water with negative staining. (b) TEM image of **F-TSC5P** in phosphate-buffered saline (PBS, 10 mM, pH = 7.4) with negative staining. The sample was prepared by dropping of the solution on an ultrathin carbon film. ([**F-TSC5P**] = 500 μM, scale bar: 100 nm).

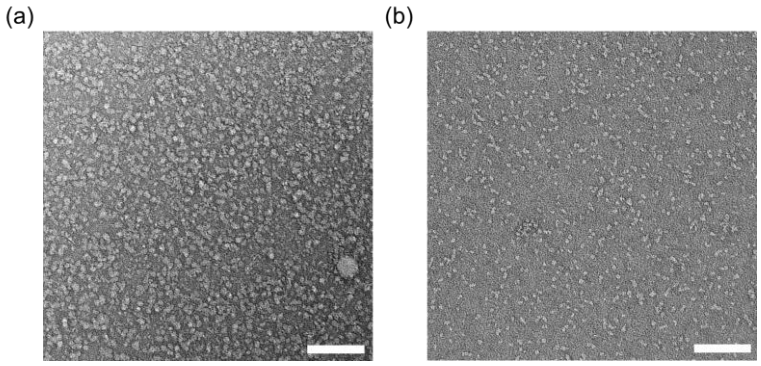

Figure S14. (a) TEM image of **TSC8P** in deionized water with negative staining. (b) TEM image of **TSC8P** in phosphate-buffered saline (PBS, 10 mM, pH = 7.4) with negative staining. The sample was prepared by dropping of the solution on an ultrathin carbon film. ([**TSC8P**] = 500 μM, scale bar: 100 nm).

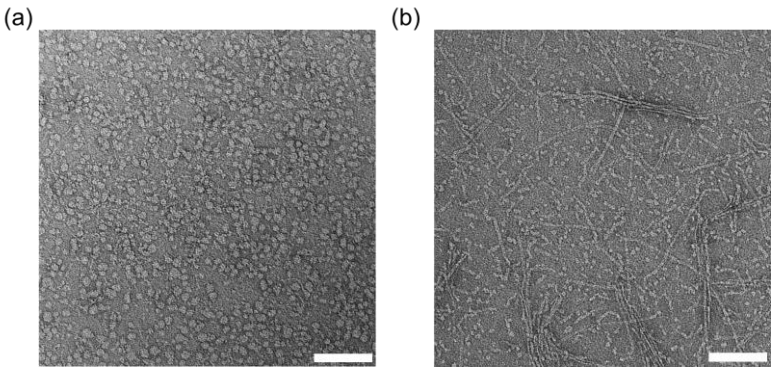

Figure S15. (a) TEM image of **TSC7P** in deionized water with negative staining. (b) TEM image of **TSC7P** in phosphate-buffered saline (PBS, 10 mM, pH = 7.4) with negative staining. The sample was prepared by dropping of the solution on an ultrathin carbon film. ([**TSC7P**] = 500 μM, scale bar: 100 nm).

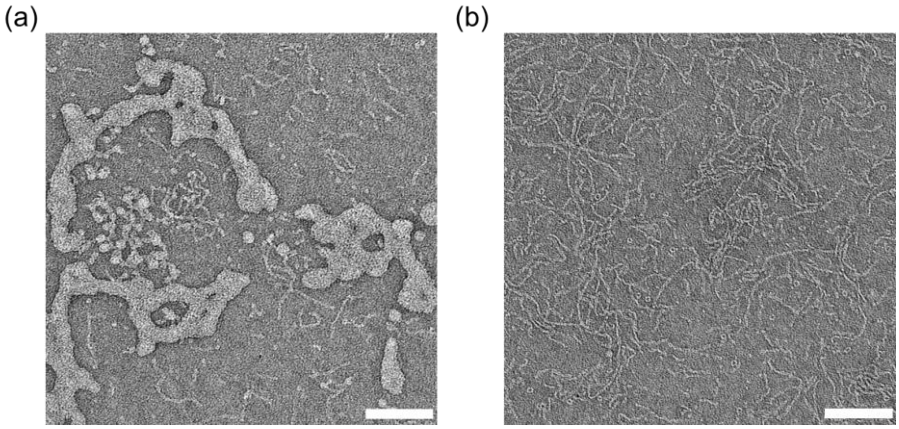

Figure S16. (a) TEM image of **TSC6P** in deionized water with negative staining. (b) TEM image of **TSC6P** in phosphate-buffered saline (PBS, 10 mM, pH = 7.4) with negative staining. The sample was prepared by dropping of the solution on an ultrathin carbon film. ([**TSC6P**] = 500 μM, scale bar: 100 nm).

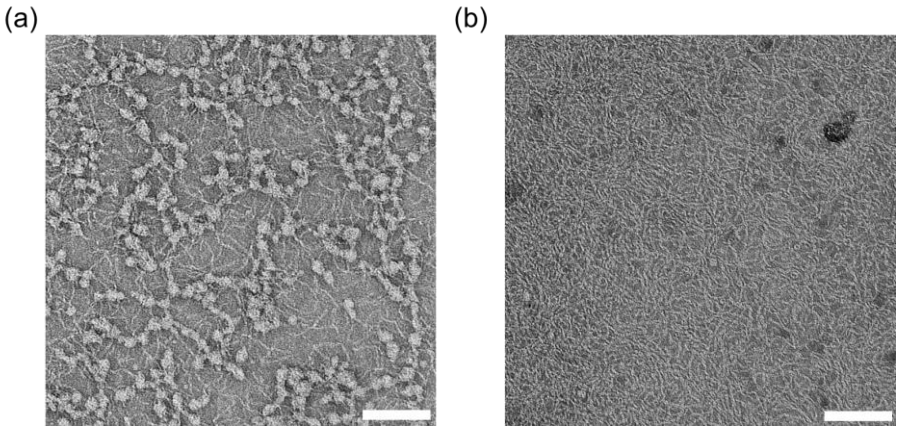

Figure S17. (a) TEM image of **TSC5P** in deionized water with negative staining. (b) TEM image of **TSC5P** in phosphate-buffered saline (PBS, 10 mM, pH = 7.4) with negative staining. The sample was prepared by dropping of the solution on an ultrathin carbon film. ([**TSC5P**] = 500 μM, scale bar: 100 nm).

CLSM images

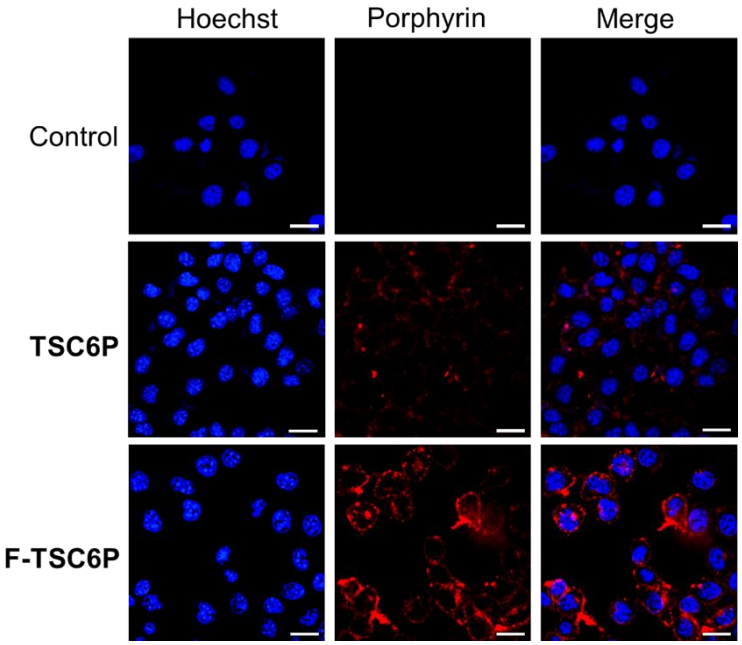

Figure S18. CLSM images (scale bar = 20 μm) of B16-F10 cells after treatment with blank medium, **TSC6P** or **F-TSC6P** (both 20.0 μM) for 4 h at 37 °C. Cell nucleus (λ_{ex} = 405 nm, λ_{em} = 460/50 nm) and porphyrin (λ_{ex} = 561 nm, λ_{em} = 700/75 nm) are showed in blue and red, respectively.

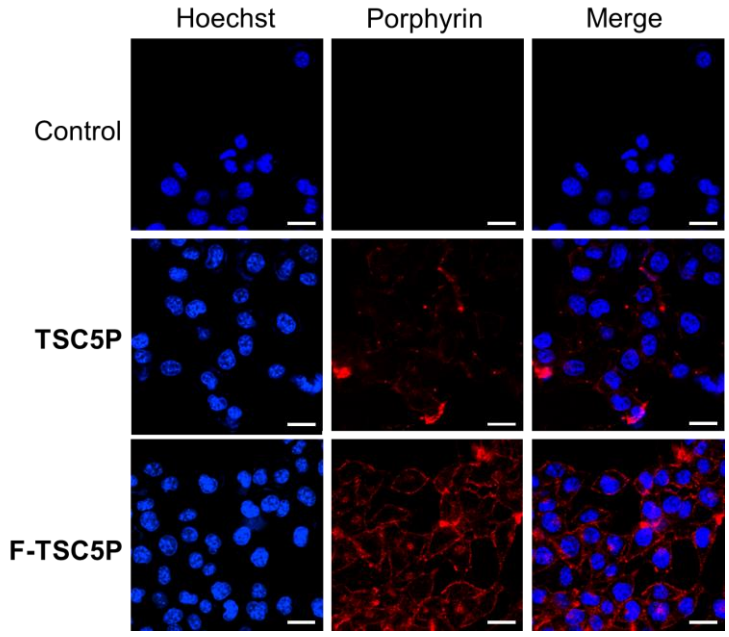

Figure S19. CLSM images (scale bar = 20 μm) of B16-F10 cells after treatment with blank medium, **TSC5P** or **F-TSC5P** (both 20.0 μM) for 4 h at 37 °C. Cell nucleus (λ_{ex} = 405 nm, λ_{em} = 460/50 nm) and porphyrin (λ_{ex} = 561 nm, λ_{em} = 700/75 nm) are showed in blue and red, respectively.

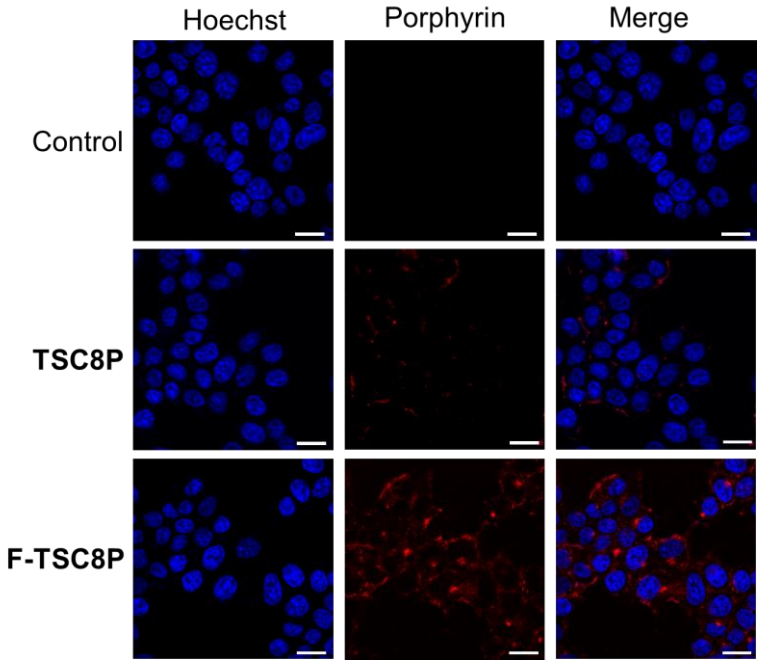

Figure S20. CLSM images (scale bar = 20 μm) of MCF-7 cells after treatment with blank medium, **TSC8P** or **F-TSC8P** (both 20.0 μM) for 4 h at 37 ℃. Cell nucleus (λ_{ex} = 405 nm, λ_{em} = 460/50 nm) and porphyrin (λ_{ex} = 561 nm, λ_{em} = 700/75 nm) are showed in blue and red, respectively.

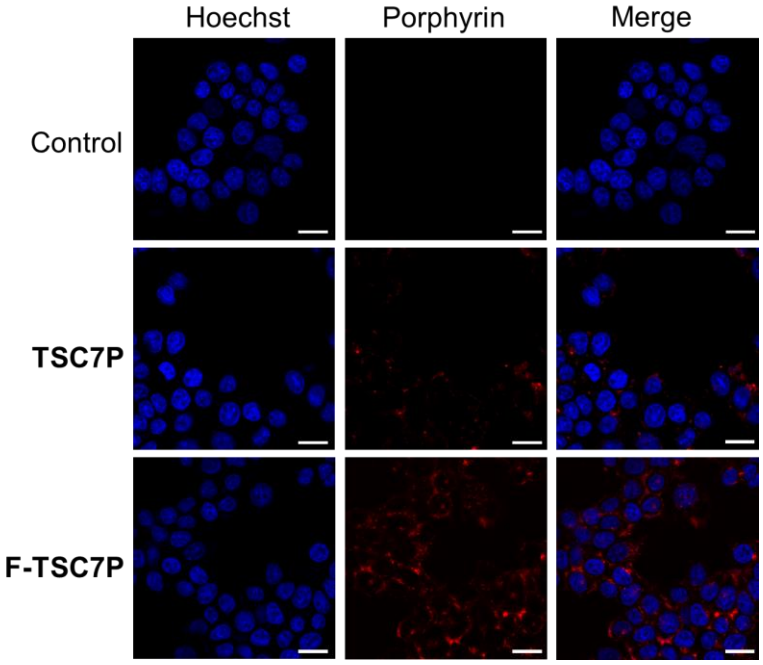

Figure S21. CLSM images (scale bar = 20 μm) of MCF-7 cells after treatment with blank medium, **TSC7P** or **F-TSC7P** (both 20.0 μM) for 4 h at 37 ℃. Cell nucleus (λ_{ex} = 405 nm, λ_{em} = 460/50 nm) and porphyrin (λ_{ex} = 561 nm, λ_{em} = 700/75 nm) are showed in blue and red, respectively.

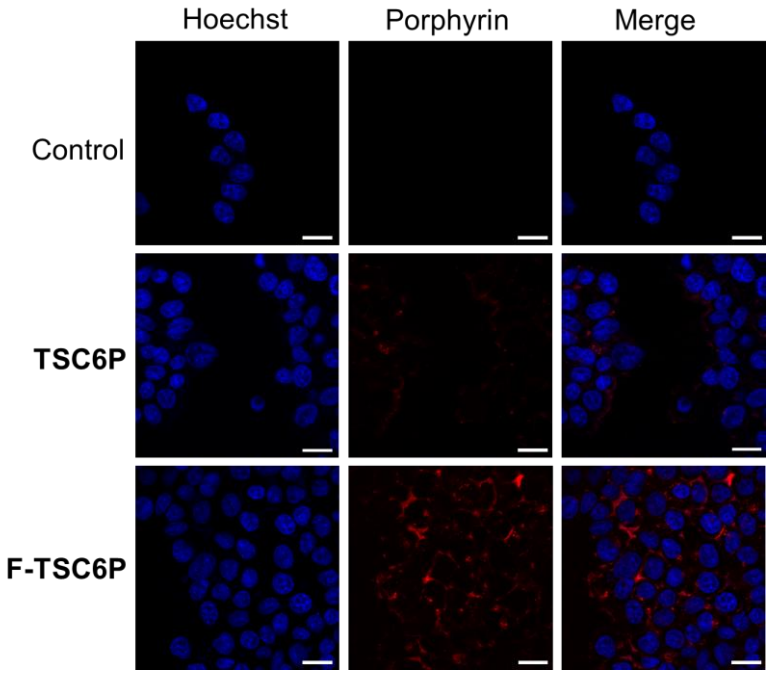

Figure S22. CLSM images (scale bar = 20 μm) of MCF-7 cells after treatment with blank medium, **TSC6P** or **F-TSC6P** (both 20.0 μM) for 4 h at 37 ℃. Cell nucleus (λ_{ex} = 405 nm, λ_{em} = 460/50 nm) and porphyrin (λ_{ex} = 561 nm, λ_{em} = 700/75 nm) are showed in blue and red, respectively.

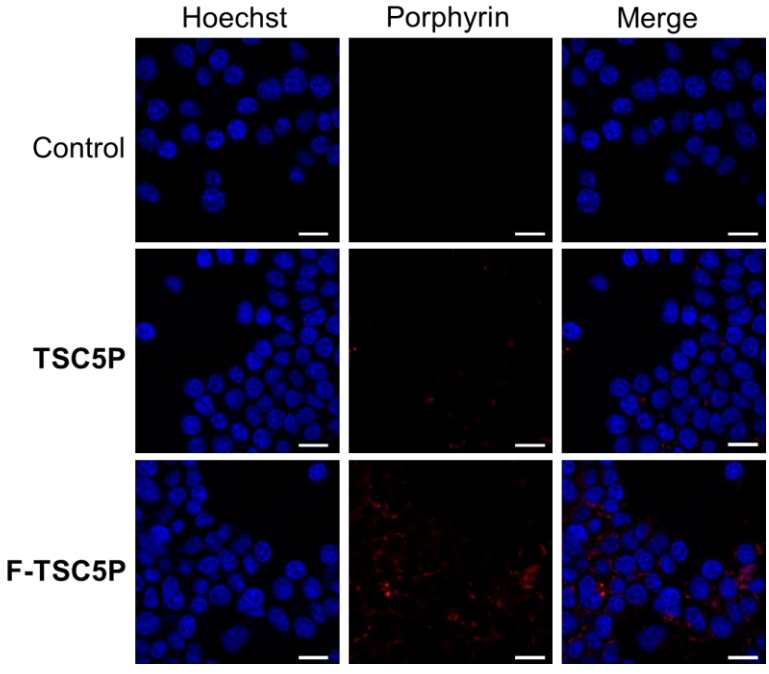

Figure S23. CLSM images (scale bar = 20 μm) of MCF-7 cells after treatment with blank medium, **TSC5P** or **F-TSC5P** (both 20.0 μM) for 4 h at 37 ℃. Cell nucleus (λ_{ex} = 405 nm, λ_{em} = 460/50 nm) and porphyrin (λ_{ex} = 561 nm, λ_{em} = 700/75 nm) are showed in blue and red, respectively.

Fluorescence intensity summary

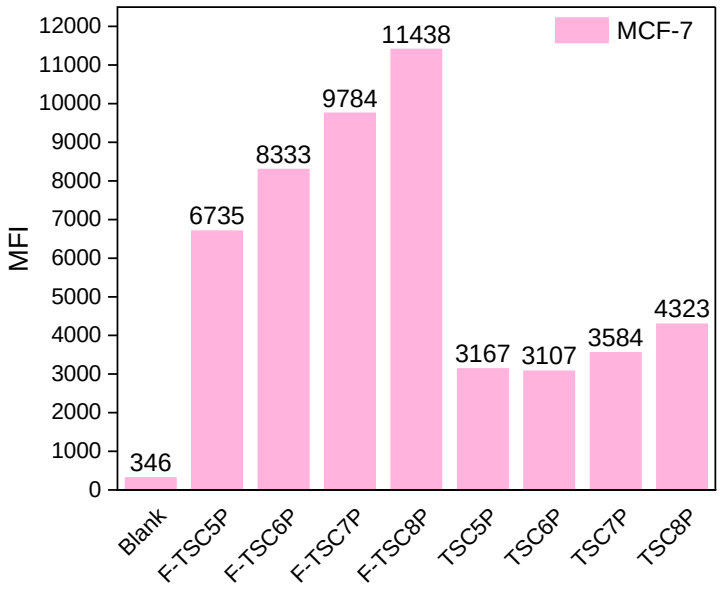

Figure S24. Mean fluorescence intensity of **F-TSCnP** (n = 5-8) and **TSCnP** (n = 5-8) (both 20 μM) in MCF-7 cancer cells determined by flow cytometry (Y675 channel: $\lambda_{excitation}$ = 561 nm, $\lambda_{emission}$ = 675/30 nm).

Fluorescence and UV-vis absorption spectra

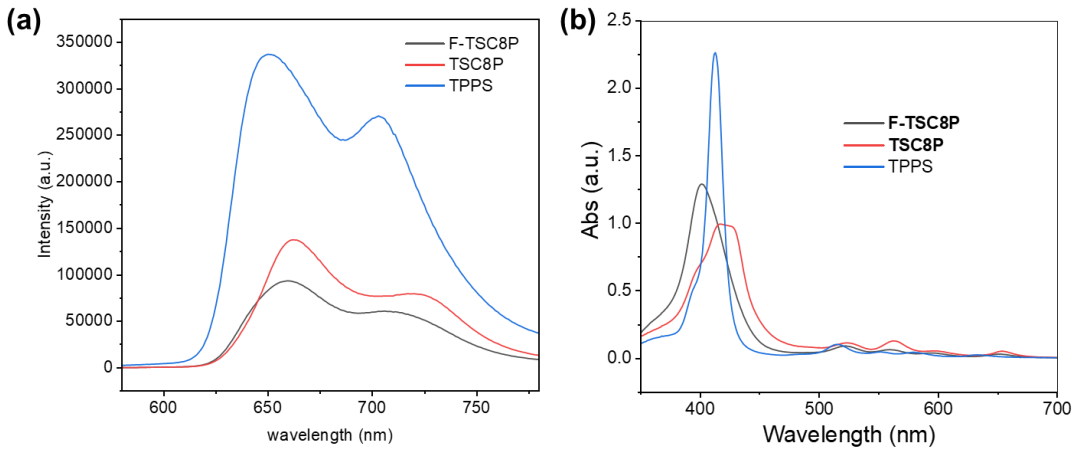

Figure S25. (a) Photoluminescence spectra of TPPS (blue), **TSC8P** (red) and **F-TSC8P** (black) (all 10.0 μM) in PBS (10 mM, pH = 7.4) at 25 °C (λ_{ex} = 415 nm). All the solutions were left to stand for 24 h before measurement. (b) UV-vis spectra of TPPS (blue), **TSC8P** (red) or **F-TSC8P** (black) (all 10.0 μM) in PBS (10 mM, pH = 7.4) at 25 °C. All the solutions were left to stand for 24 h before measurement.

Oxygen release profile

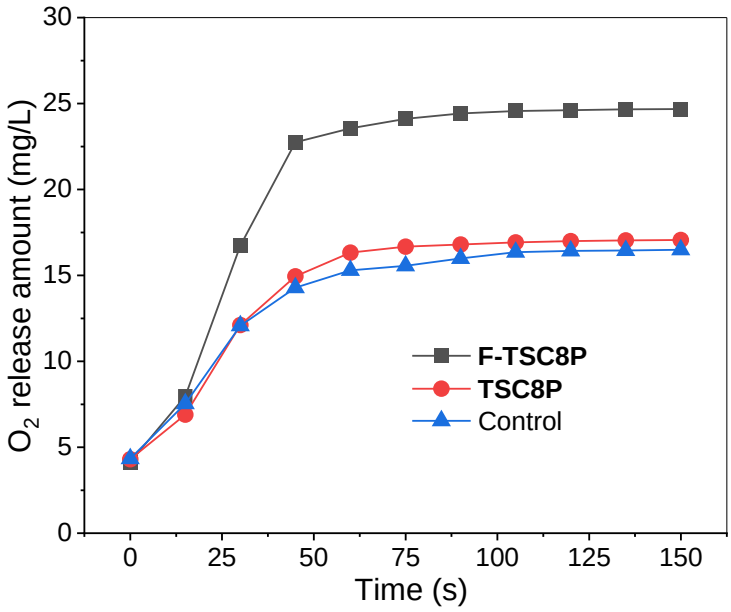

Figure S26. Time-dependent O_2 release from the PBS solution of **F-TSC8P** and **TSC8P** (both 40 μM), and O_2-saturated PBS solution.

UV-vis absorption spectra

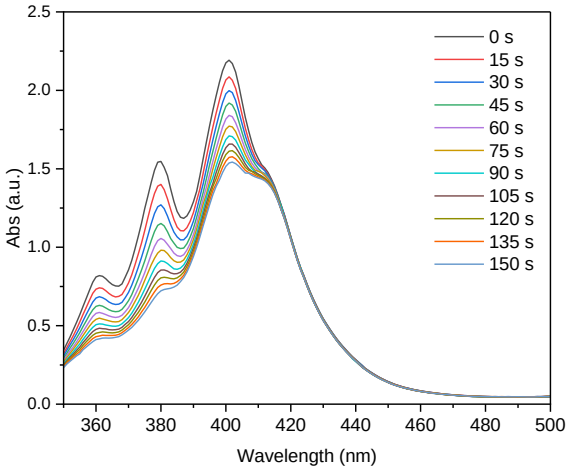

Figure S27. Changes in UV-vis spectra of ABDA (100 μM) in PBS (10 mM, pH = 7.4) containing 10 μM **F-TSC8P** at 25 ℃ after laser irradiation (655 nm, 0.2 W/cm^2) of different time intervals.

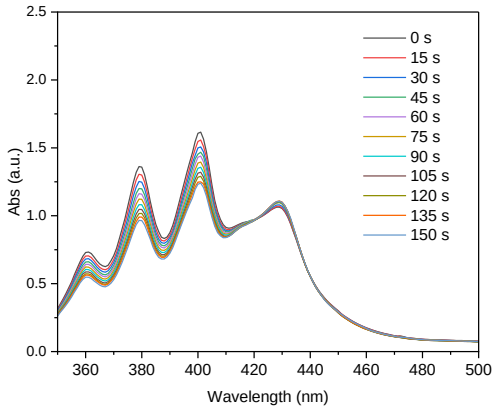

Figure S28. Changes in UV-vis spectra of ABDA (100 μM) in PBS (10 mM, pH = 7.4) containing 10 μM **F-TSC8P** at 25 ℃ after laser irradiation (655 nm, 0.2 W/cm^2) of different time intervals.

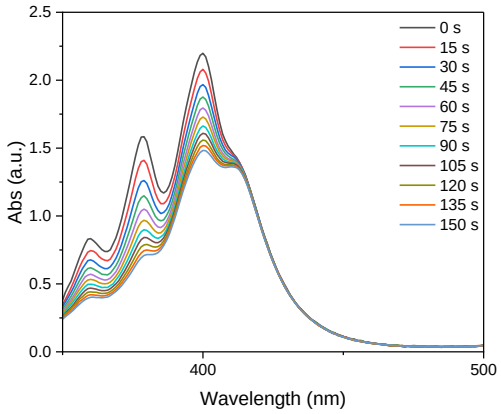

Figure S29. Changes in UV-vis spectra of ABDA (100 μM) in saline containing 10 μM **F-TSC8P** at 25 ℃ after laser irradiation (655 nm, 0.2 W/cm^2) of different time intervals.

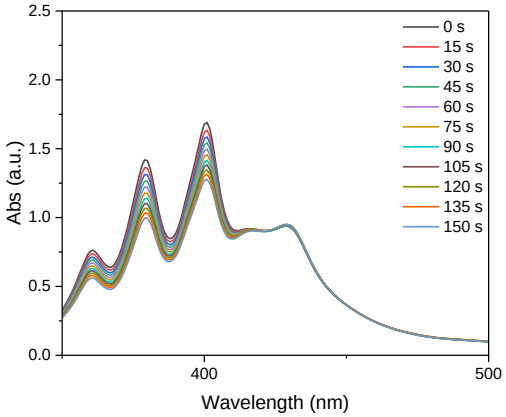

Figure S30. Changes in UV-vis spectra of ABDA (100 μM) in saline containing 10 μM **TSC8P** at 25 ℃ after laser irradiation (655 nm, 0.2 W/cm^2) of different time intervals.

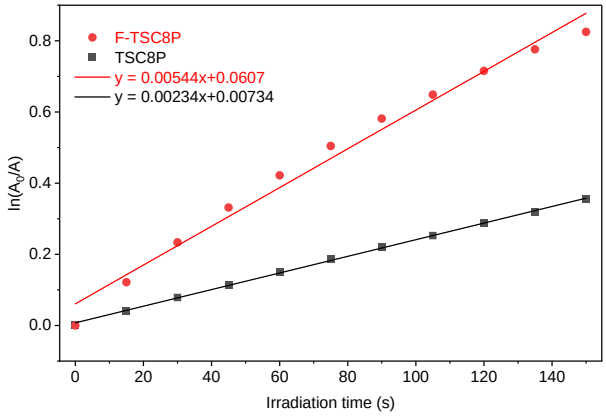

Figure S31. Time-dependent UV-vis absorbance (378 nm) changes of ABDA (0.1 mM) sensitized by **F-TSC8P** and **TSC8P** (both 10 μM) under laser irradiation (0.2 W/cm^2) in normal saline.

Fluorescence spectra

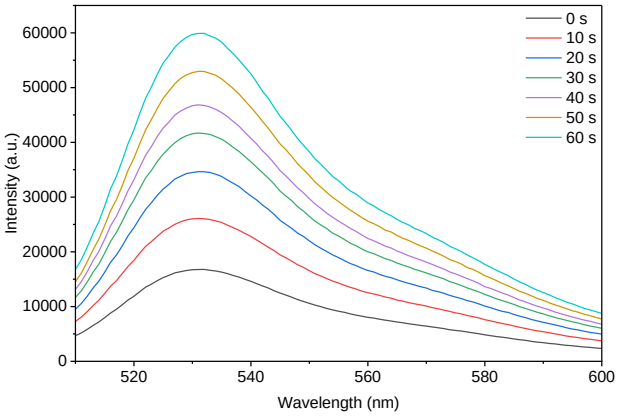

Figure S32. Changes in FL spectra of SOSG (5 μM) in PBS (10 mM, pH = 7.4) containing 5 μM **F-TSC8P** at 25 ℃ after laser irradiation (655 nm, 0.2 W/cm^2) of different time intervals.

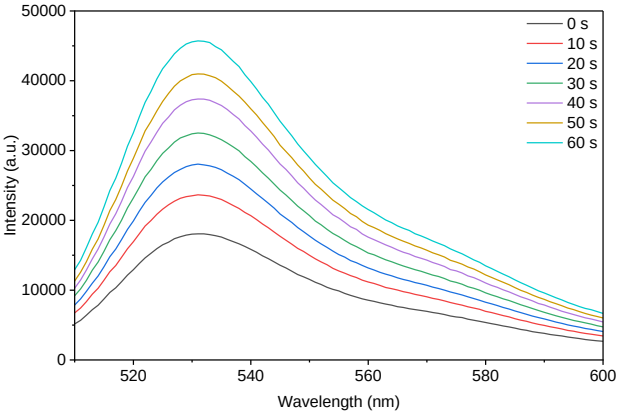

Figure S33. Changes in FL spectra of SOSG (5 μM) in PBS (10 mM, pH = 7.4) containing 5 μM **TSC8P** at 25 ℃ after laser irradiation (655 nm, 0.2 W/cm^2) of different time intervals.

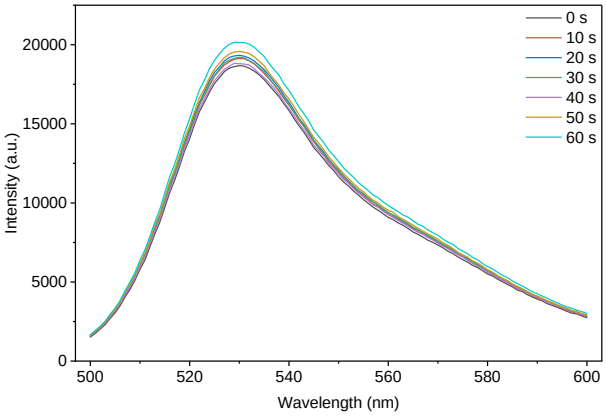

Figure S34. Changes in FL spectra of SOSG (5 μM) in PBS (10 mM, pH = 7.4) at 25 ℃ after laser irradiation (655 nm, 0.2 W/cm^2) of different time intervals.

Cell viability profiles

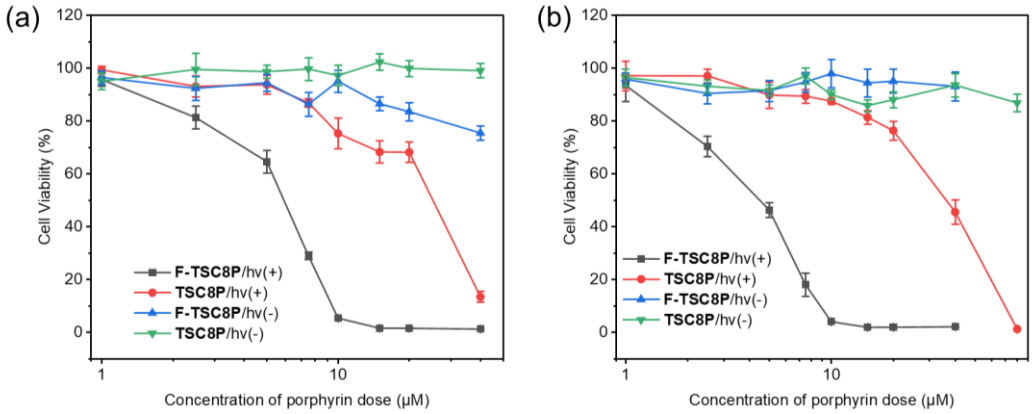

Figure S35. Viability of (a) normal B16-F10 cells and MCF-7 cells treated with **F-TSC8P** (1.0-40 μM) and **TSC8P** (1.0-80 μM) of variable concentrations with or without laser irradiation (50 mW/cm^2, 60 J/cm^2, 20 min).

In vivo model procedure

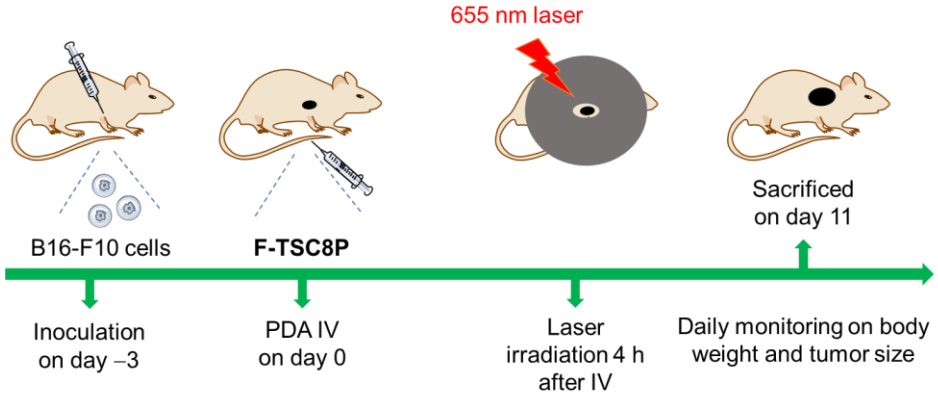

Figure S36. Schematic illustration of the in vivo assessment of the PDT activity for inhibiting the **F-TSC8P** tumor with mouse model.

Organ tissue imaging

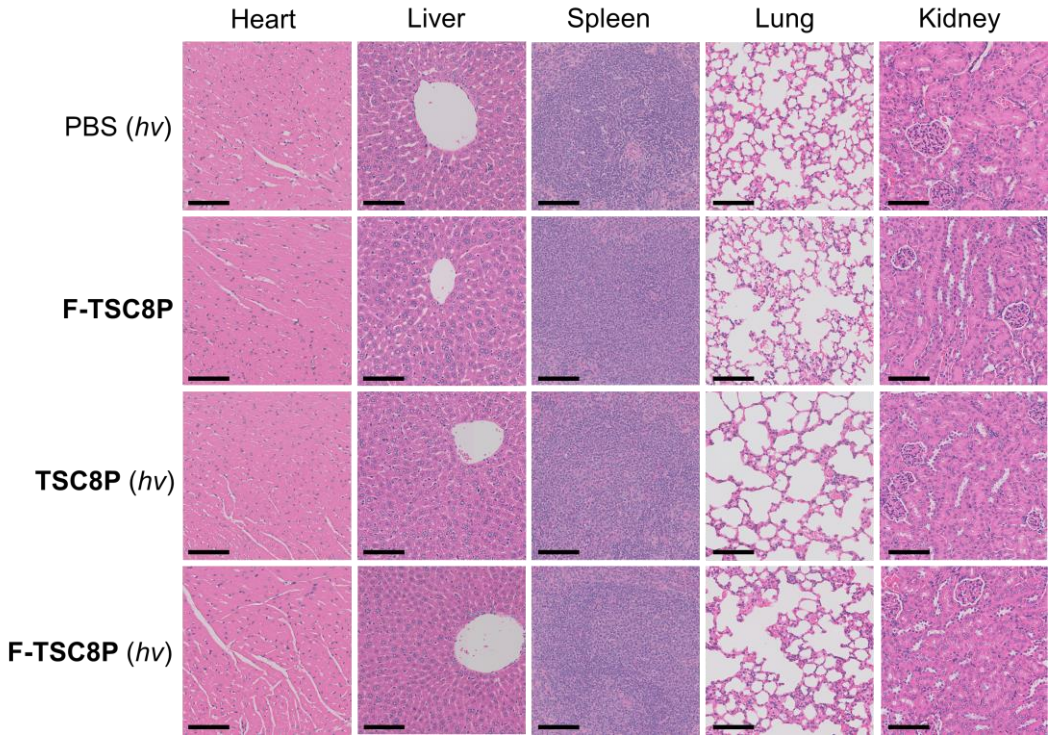

Figure S37. H&E staining images of major organs (heart, liver, spleen, lung and kidney) collected from each group of the mice implanted with B16-F10 tumor (scale bar: 100 μm).

Body weight profile

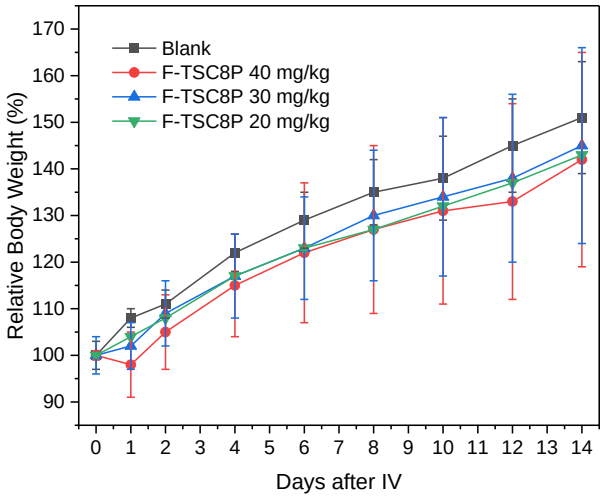

Figure S38. Relative body weight changes of mice versus the observation day after IV of **F-TSC8P** of different doses.

Organ tissue imaging

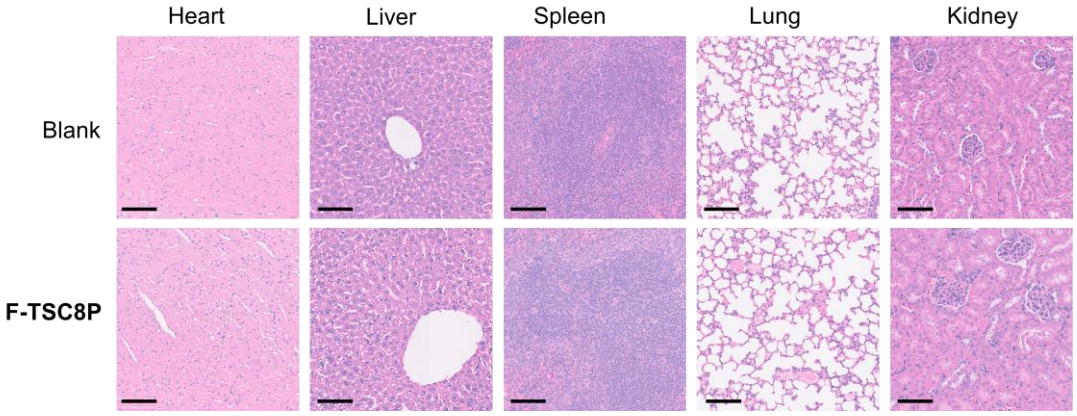

Figure S39. H&E staining images of major organs (heart, liver, spleen, lung and kidney) collected from each group (scale bar: 100 μm).

Cell viability profiles

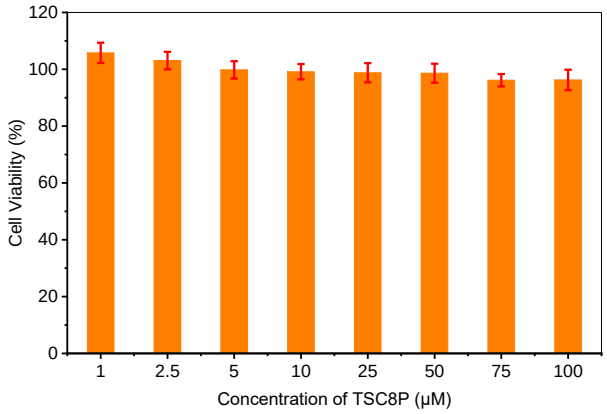

Figure S40. Viability of H9C2 cells treated with **F-TSC8P** of different concentrations.

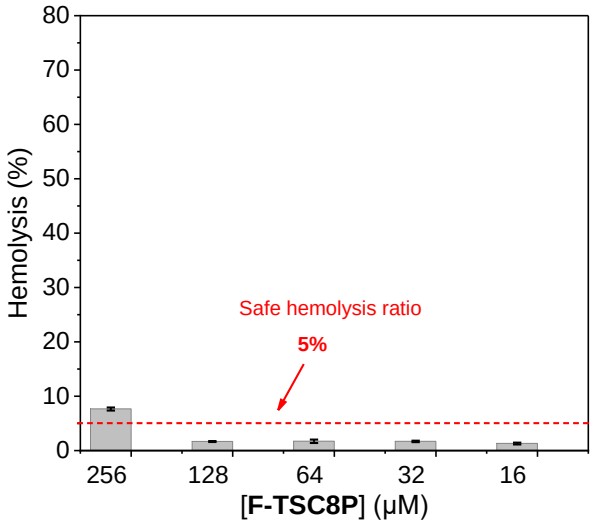

Figure S41. Hemolysis ratio of SD rat erythrocytes treated with **F-TSC8P** of variable concentration.

NMR spectra

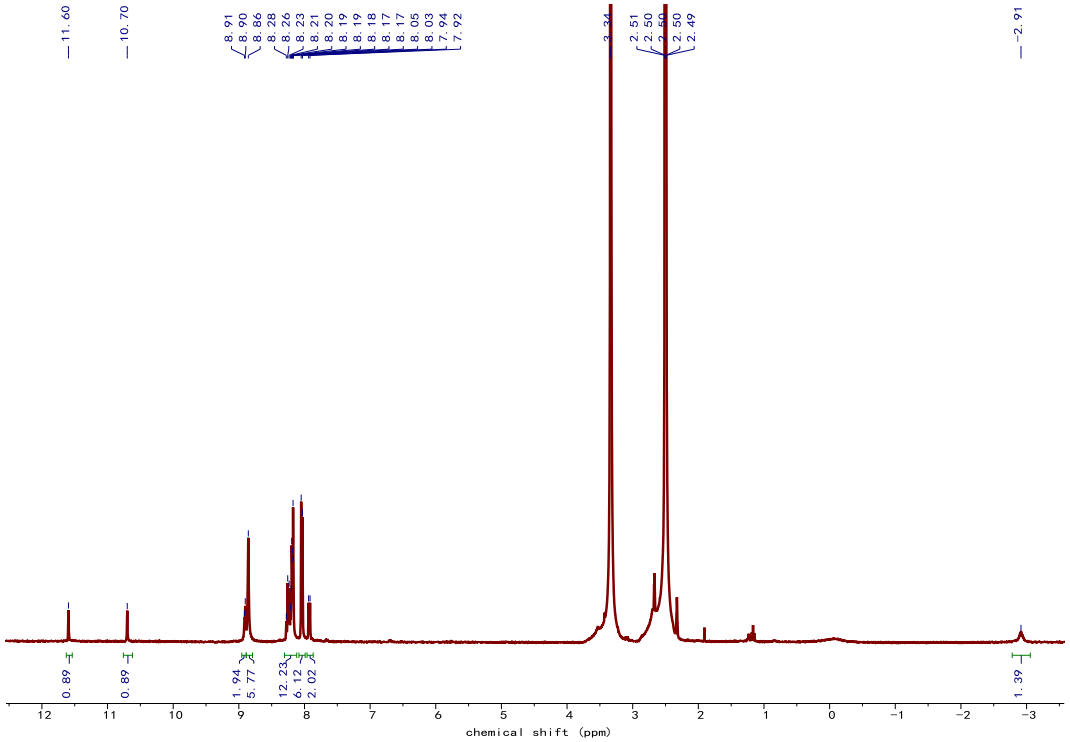

Figure S42. ^{1}H NMR spectrum (DMSO-d$_6$, 400 MHz, 298 K) of **F-TSC8P**.

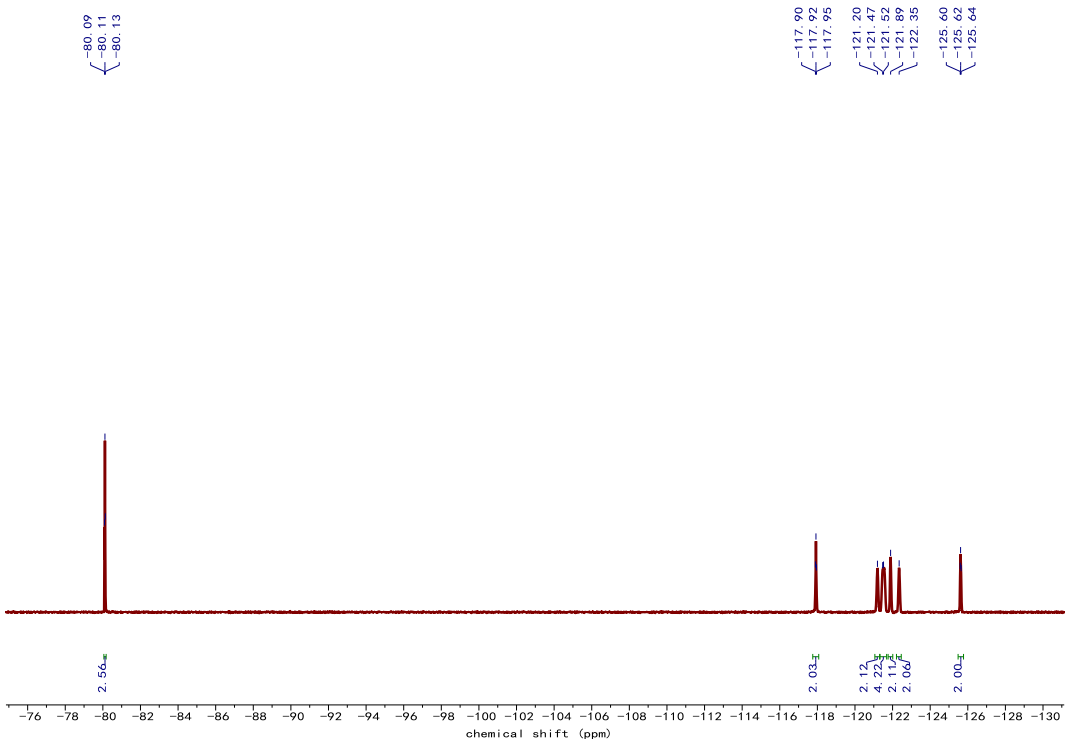

Figure S43. ^{19}F NMR spectrum (DMSO-d$_6$, 470 MHz, 298 K) of **F-TSC8P**.

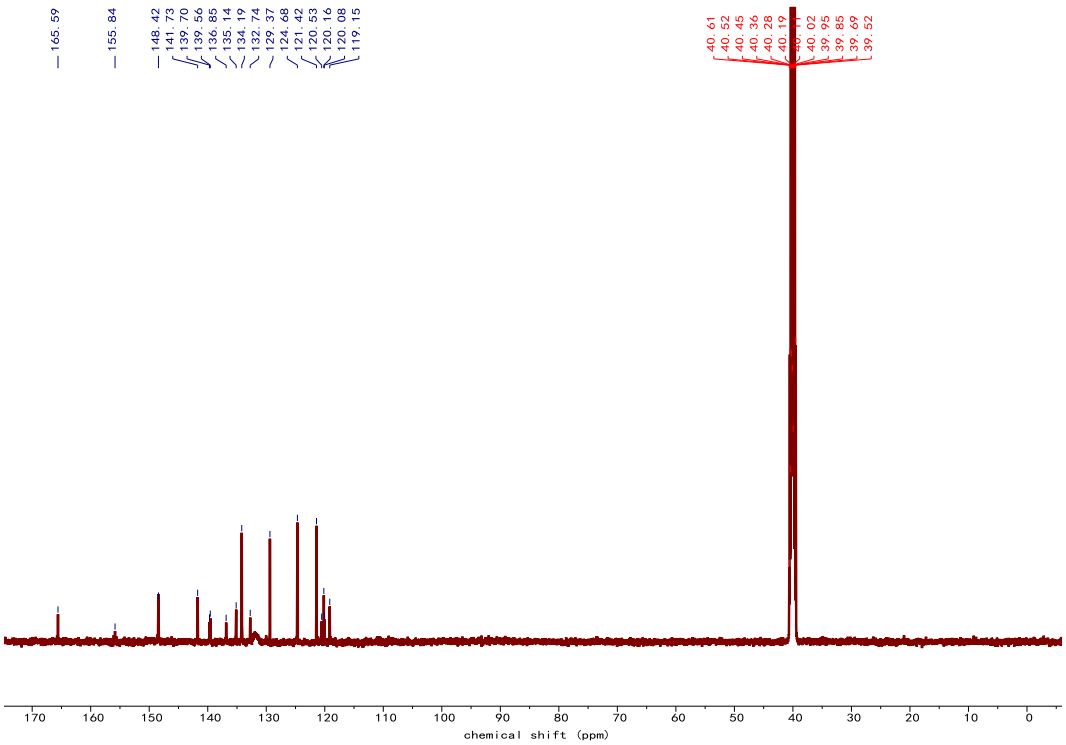

Figure S44. ^{13}C NMR spectrum (DMSO-d$_6$, 125 MHz, 298 K) of **F-TSC8P**.

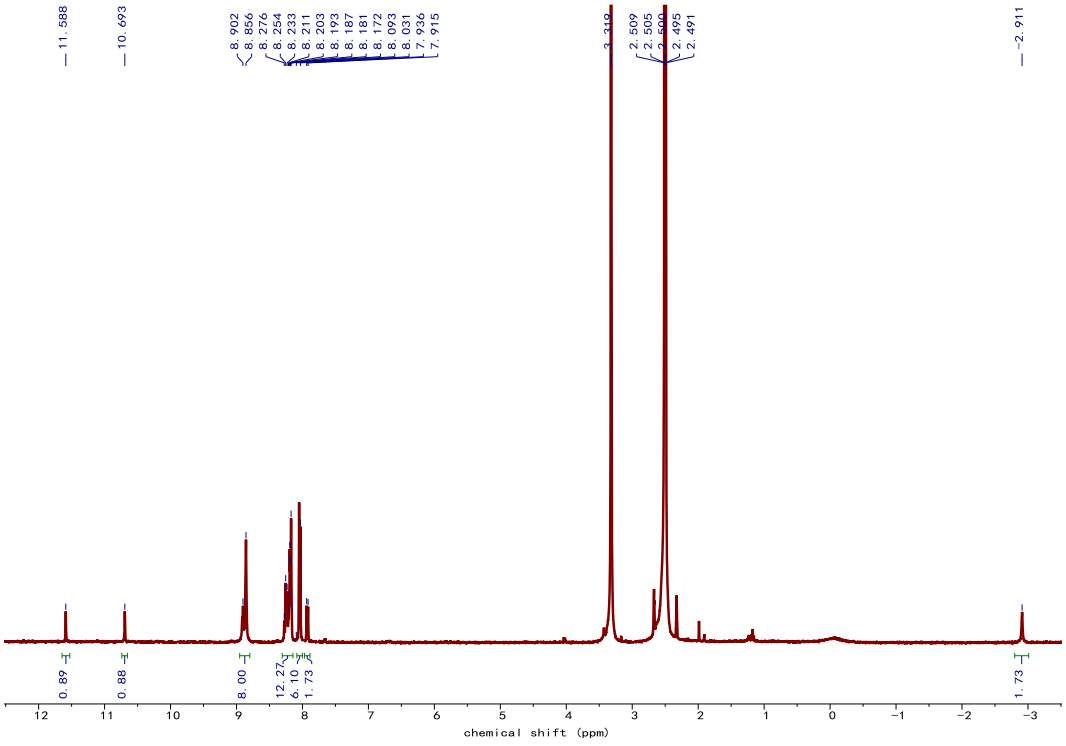

Figure S45. ^{1}H NMR spectrum (DMSO-d$_6$, 400 MHz, 298 K) of **F-TSC7P**.

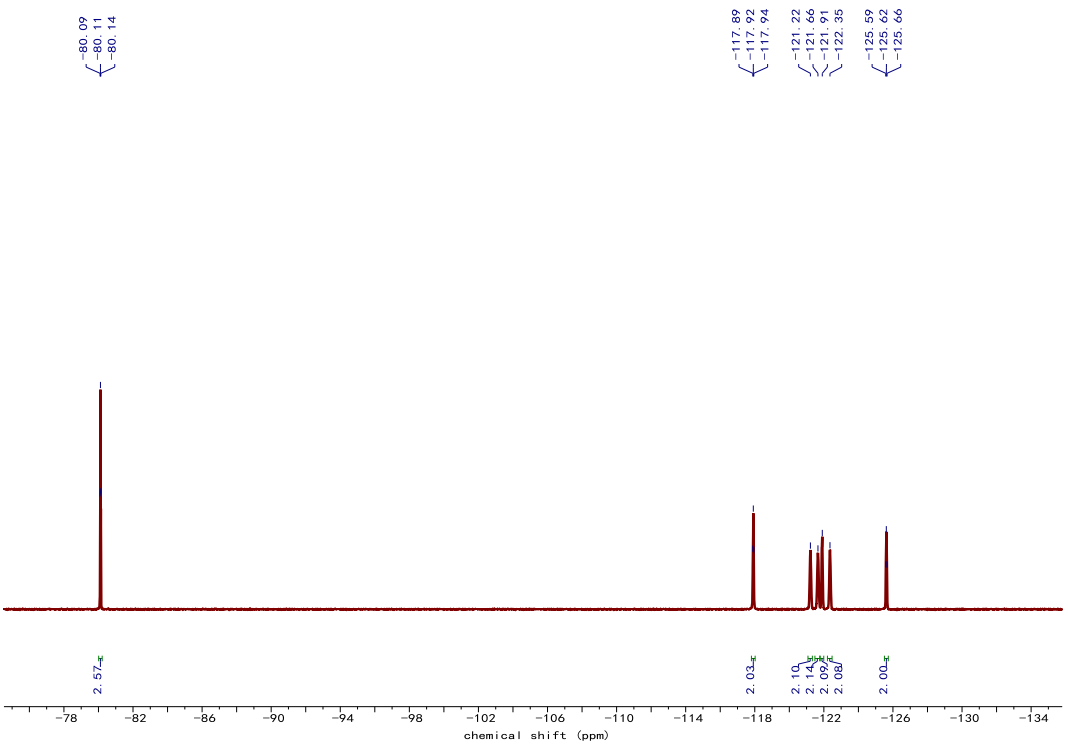

Figure S46. ^{19}F NMR spectrum (DMSO-d$_6$, 470 MHz, 298 K) of **F-TSC7P**.

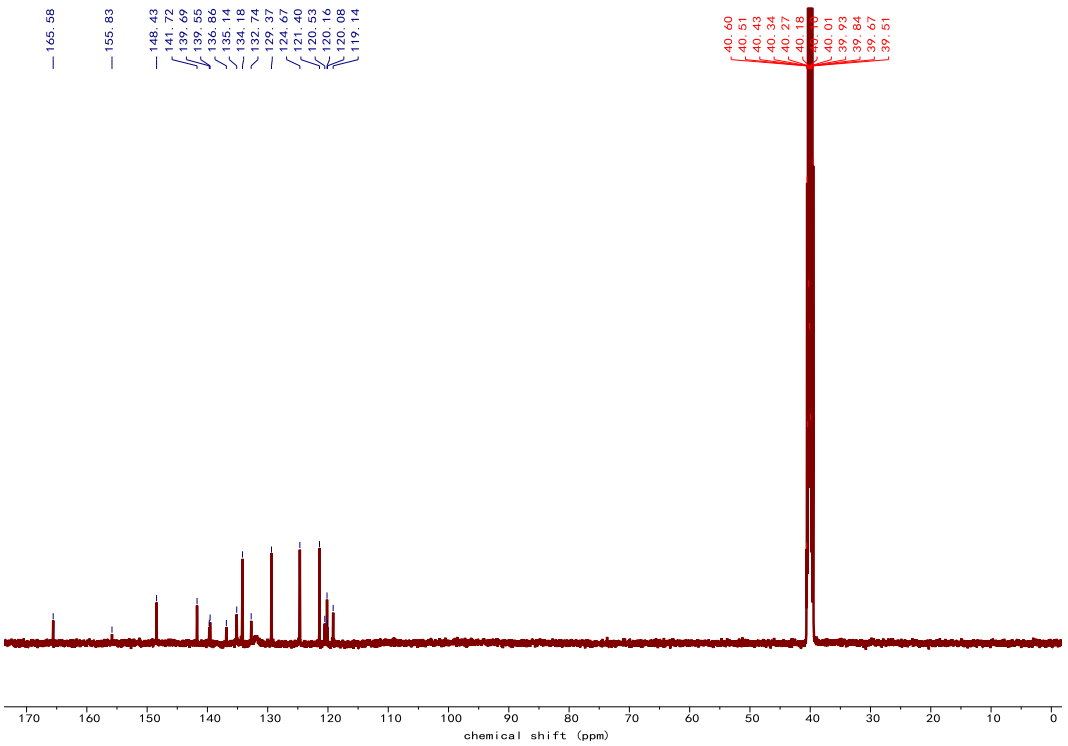

Figure S47. ^{13}C NMR spectrum (DMSO-d$_6$, 125 MHz, 298 K) of **F-TSC7P**.

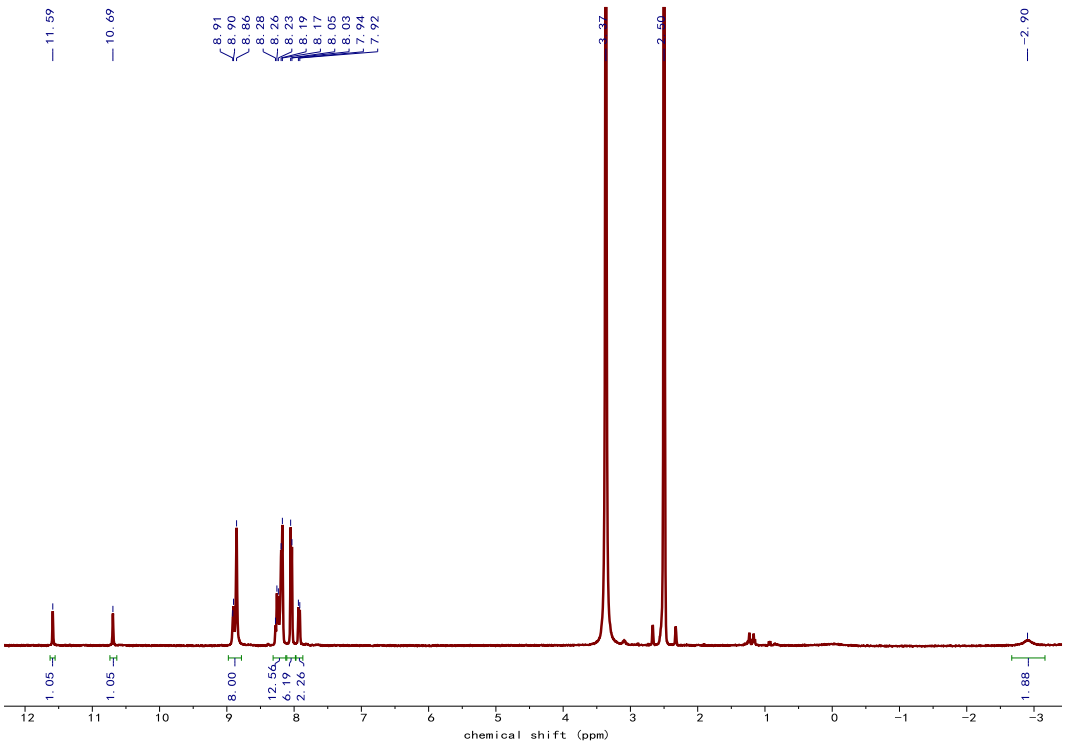

Figure S48. ^{1}H NMR spectrum (DMSO-d_6, 400 MHz, 298 K) of **F-TSC6P**.

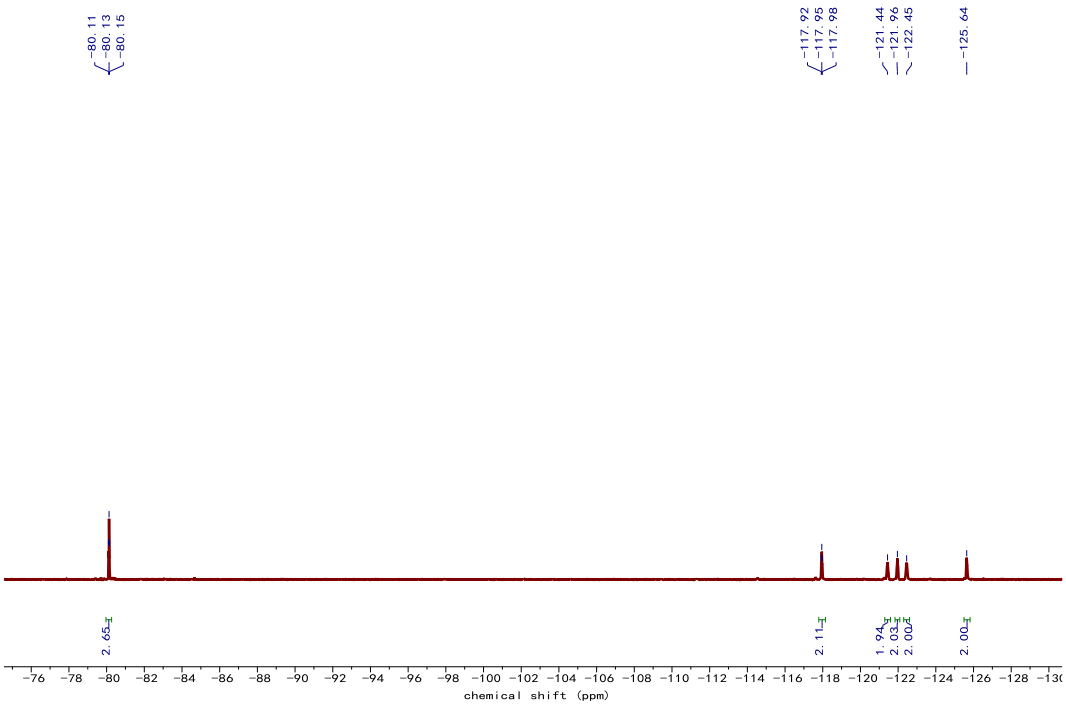

Figure S49. ^{19}F NMR spectrum (DMSO-d_6, 470 MHz, 298 K) of **F-TSC6P**.

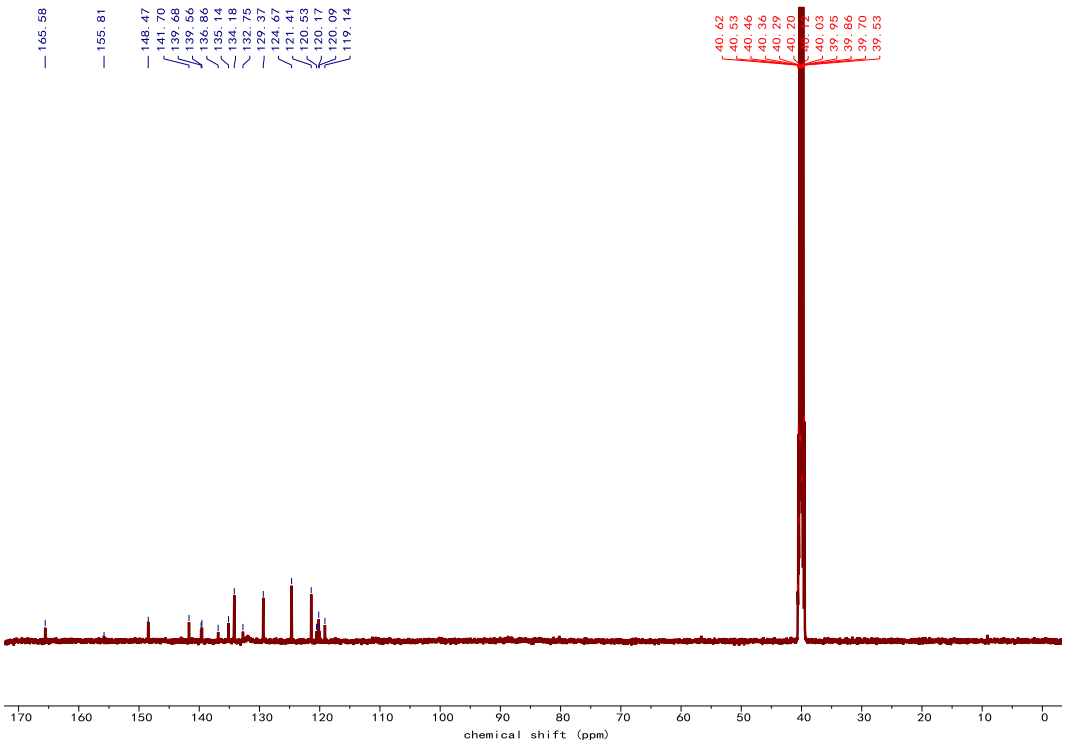

Figure S50. ^{13}C NMR spectrum (DMSO-d$_6$, 125 MHz, 298 K) of **F-TSC6P**.

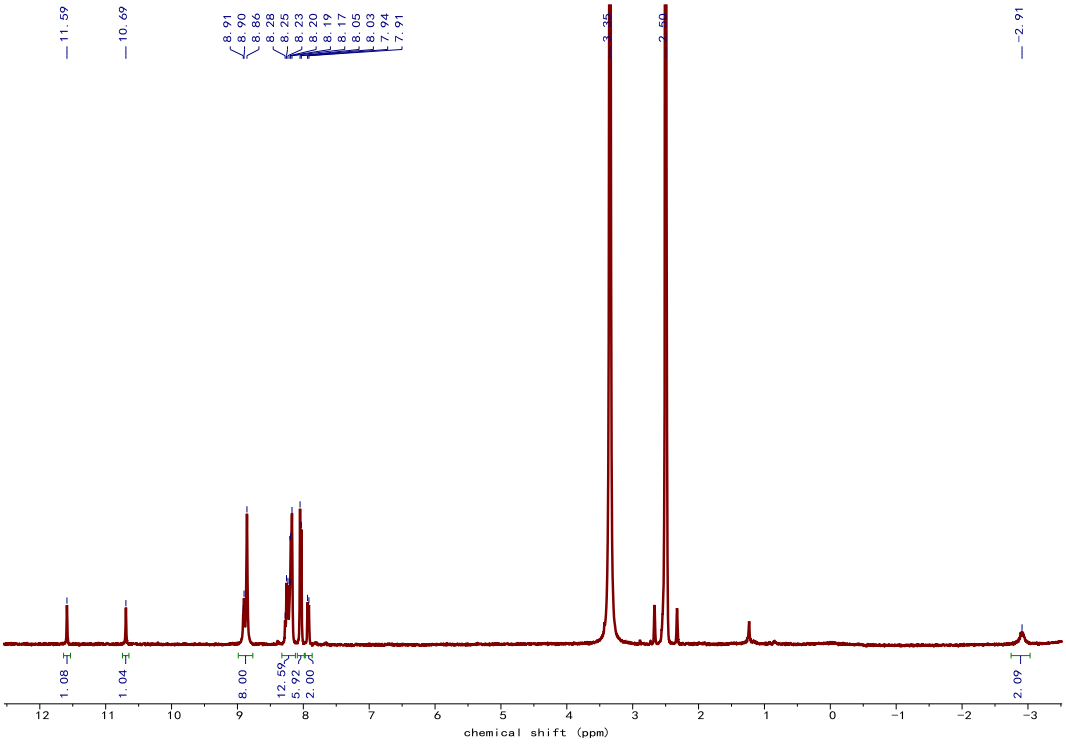

Figure S51. ^{1}H NMR spectrum (DMSO-d$_6$, 400 MHz, 298 K) of **F-TSC5P**.

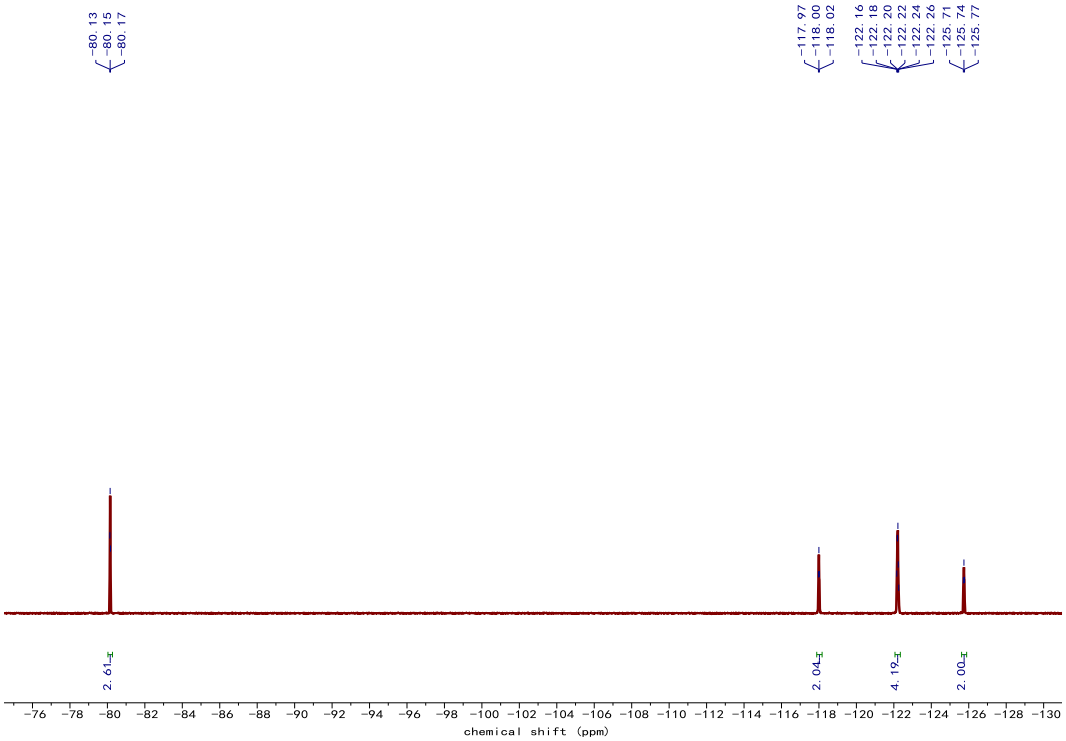

Figure S52. ^{19}F NMR spectrum (DMSO-d_6, 470 MHz, 298 K) of **F-TSC5P**.

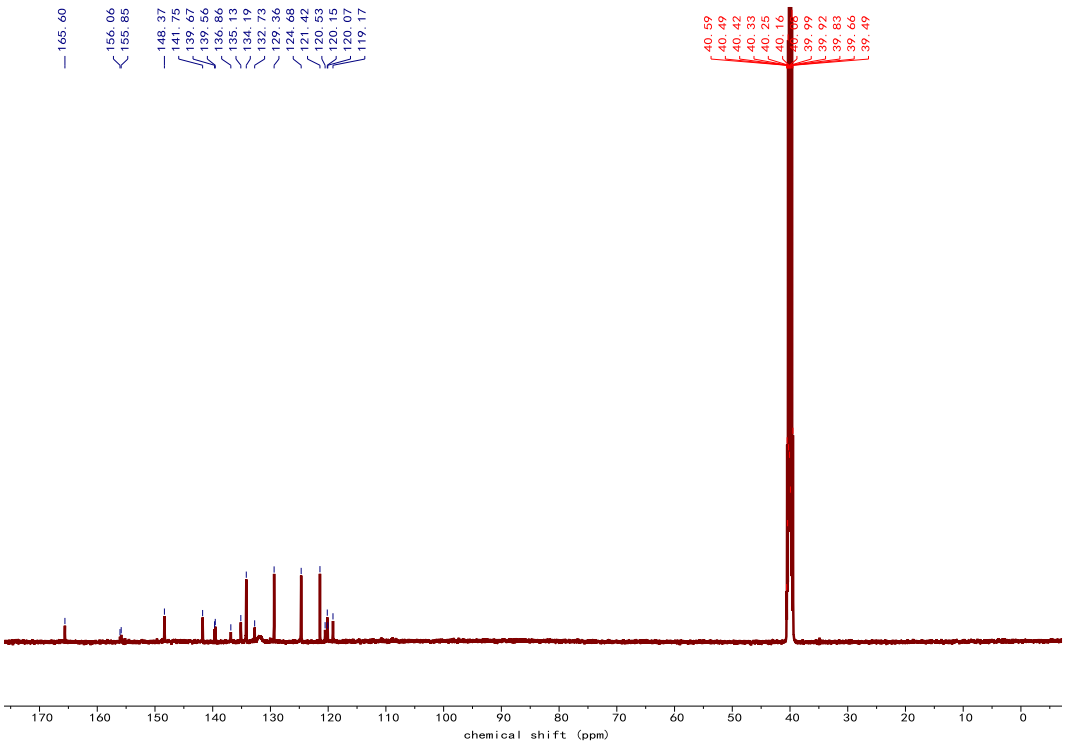

Figure S53. ^{13}C NMR spectrum (DMSO-d_6, 125 MHz, 298 K) of **F-TSC5P**.

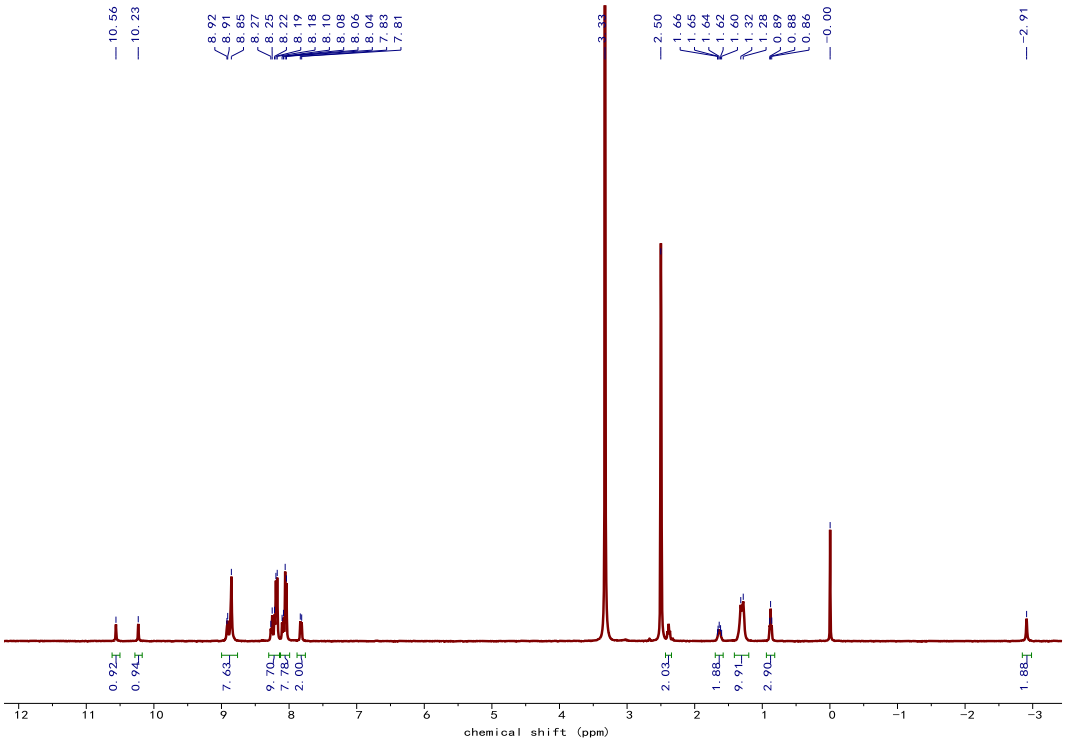

Figure S54. ^{1}H NMR spectrum (DMSO-d$_6$, 400 MHz, 298 K) of **TSC8P**.

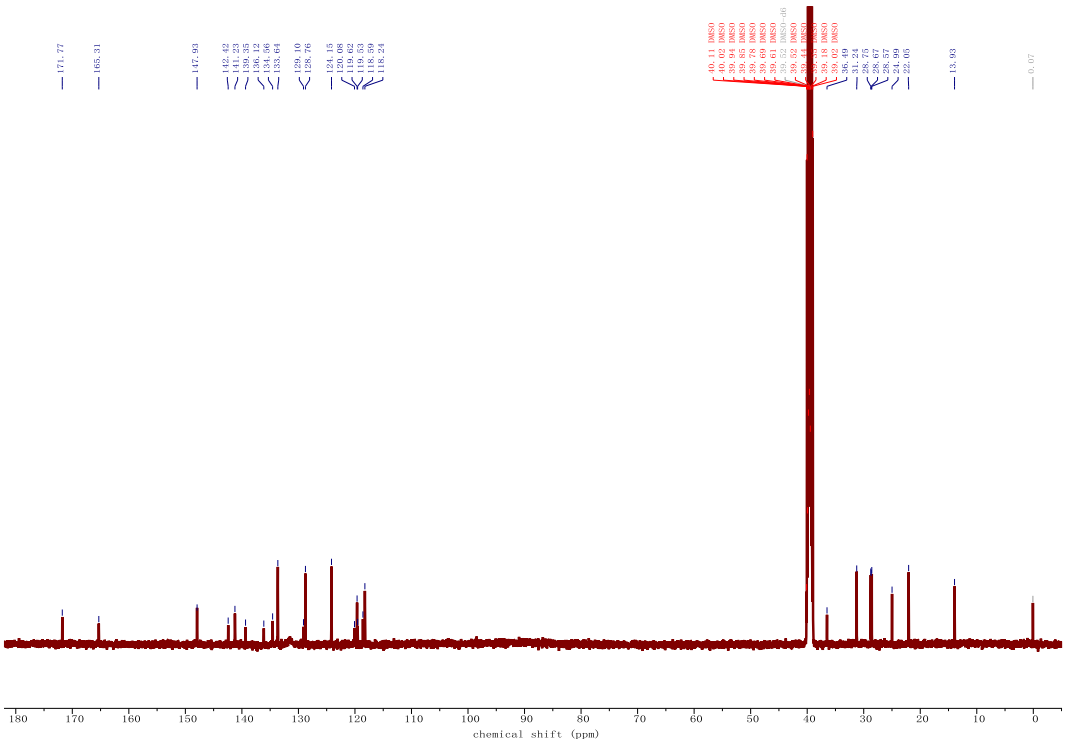

Figure S55. ^{13}C NMR spectrum (DMSO-d$_6$, 125 MHz, 298 K) of **TSC8P**.

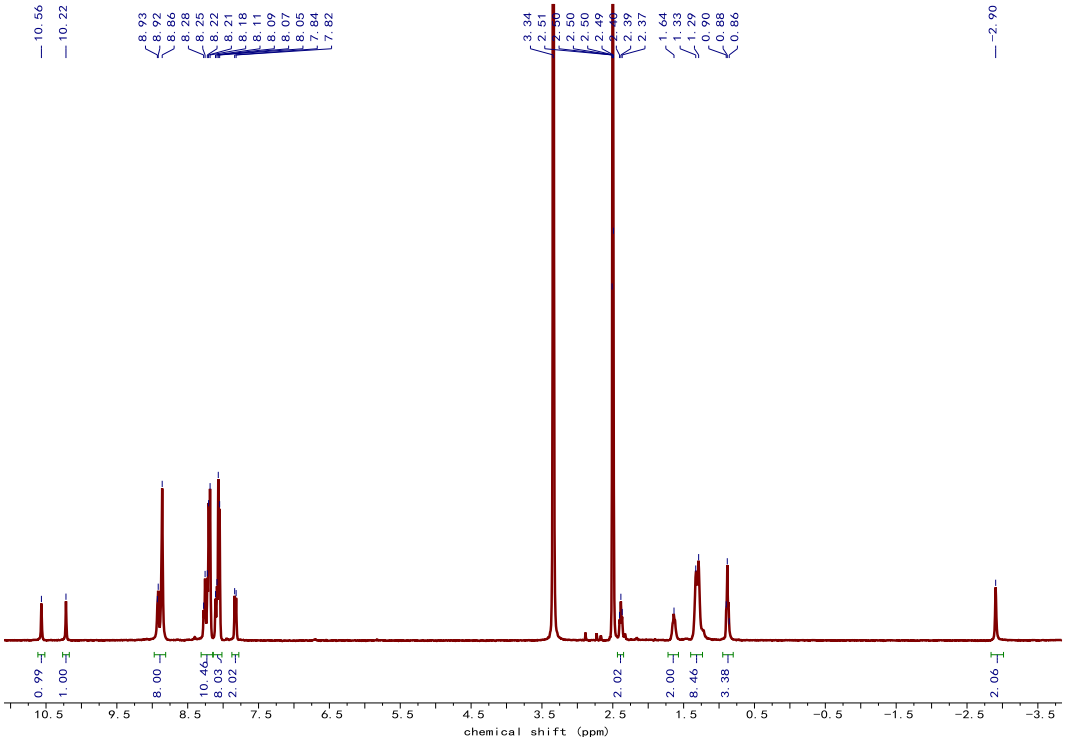

Figure S56. ^{1}H NMR spectrum (DMSO-d$_6$, 400 MHz, 298 K) of **TSC7P**.

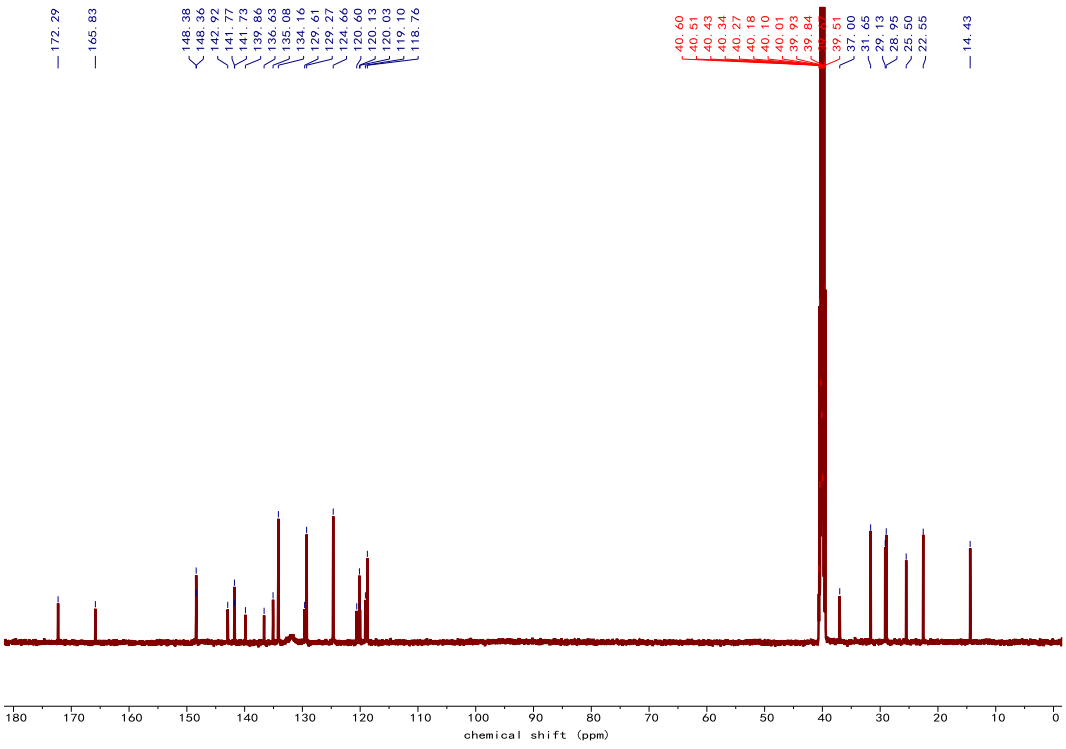

Figure S57. ^{13}C NMR spectrum (DMSO-d$_6$, 125 MHz, 298 K) of **TSC7P**.

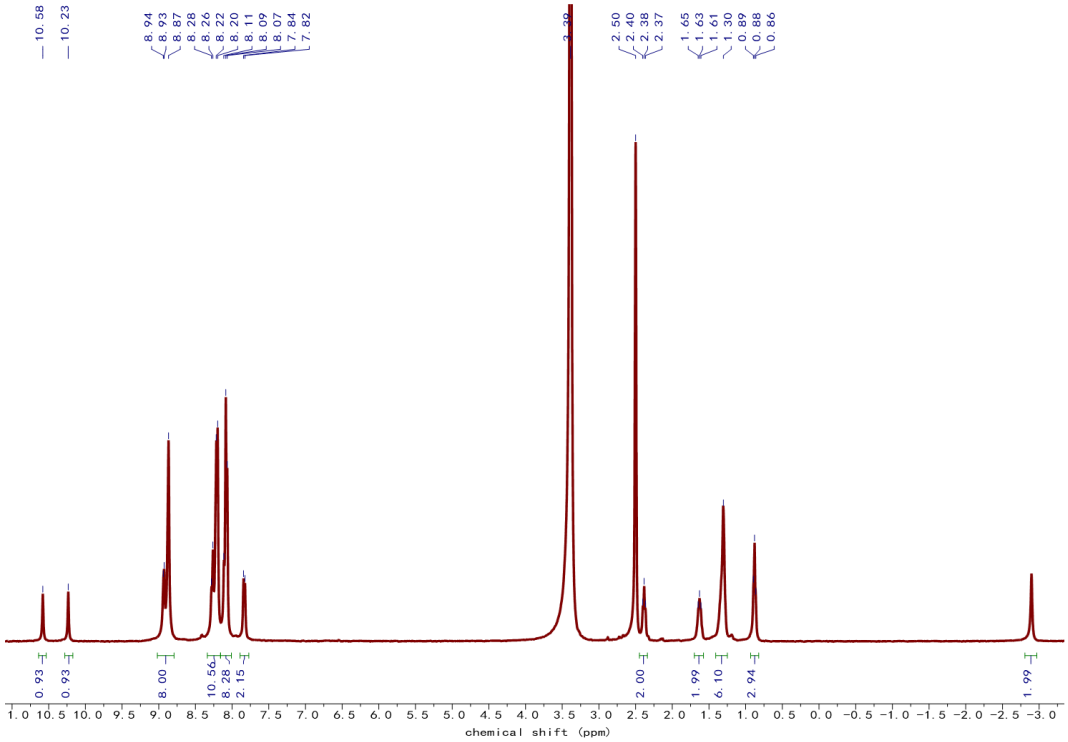

Figure S58. ^{1}H NMR spectrum (DMSO-d$_6$, 400 MHz, 298 K) of **TSC6P**.

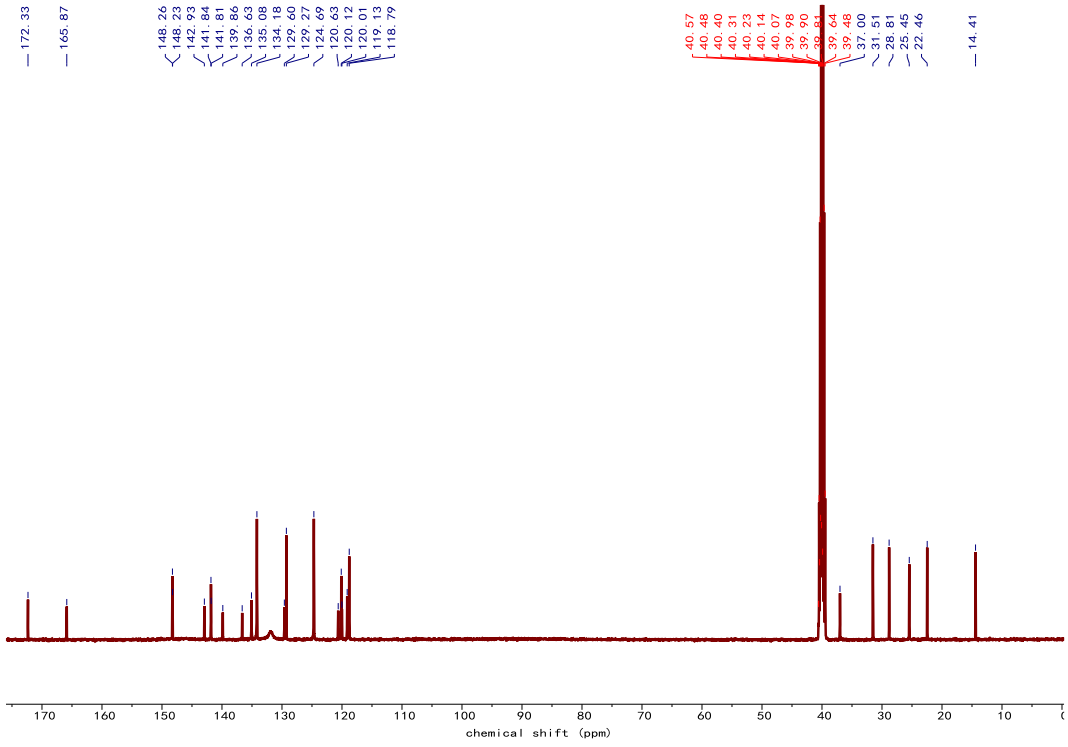

Figure S59. ^{13}C NMR spectrum (DMSO-d$_6$, 125 MHz, 298 K) of **TSC6P**.

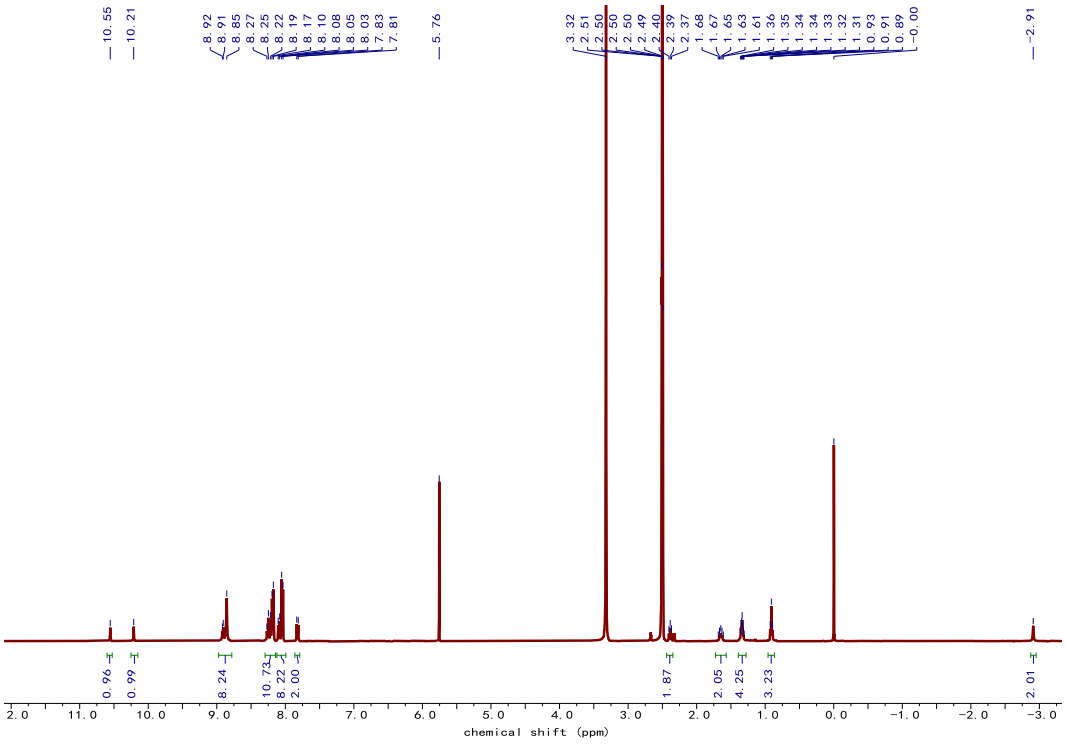

Figure S60. ^{1}H NMR spectrum (DMSO-d$_6$, 400 MHz, 298 K) of **TSC5P**.

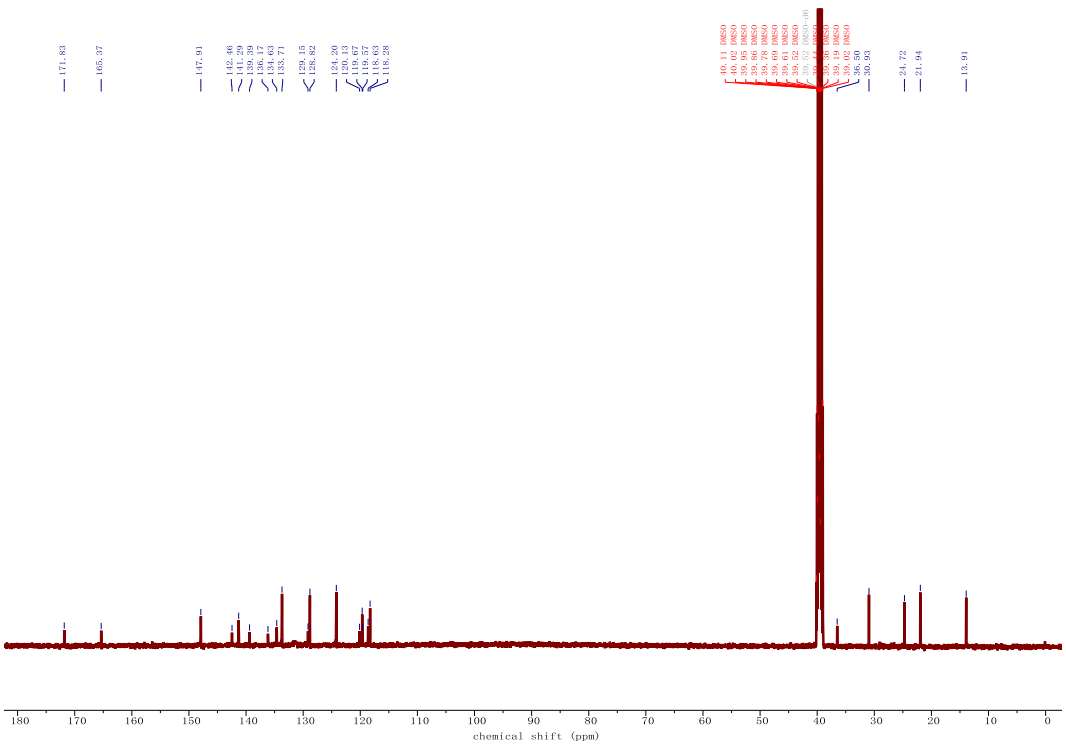

Figure S61. ^{13}C NMR spectrum (DMSO-d$_6$, 125 MHz, 298 K) of **TSC5P**.

References

1. Y.-H. Song, Y.-J. Gu, Z. Lei, N.-K. Li, Y.-M. Zhang, Q. Yu, Y. Liu, Fluorinated Cyclodextrin Supramolecular Nanoassembly Enables Oxygen-Enriched and Targeted Photodynamic Therapy, *Nano Lett.*, 2025, **25**, 4476-4484.
2. D. Ma, J. Zhang, Y.-Y. Liu, L. Zhang, Z. Zhao, Q. Lin, Y. Lei, J. Xing, H. Wang, J. Tian, D.-W. Zhang, W. Zhou, Z.-T. Li, Self-assembly of highly stable uniform single-molecule porphyrin nanomicelles for enhanced photodynamic therapy, *Sci. China Chem.*, 2025, **68**, 3660-3666.
3. H. Lin, Y. Shen, D. Chen, L. Lin, B. C. Wilson, B. Li, S. Xie, Feasibility study on quantitative measurements of singlet oxygen generation using singlet oxygen sensor green. *J. Fluoresc.*, 2013, **23**, 41-47.